actuators

MDPI

Article

Observer-Based Adaptive Neural Control of Quadrotor Unmanned Aerial Vehicles Subject to Model Uncertainties and External Disturbances

Rashin Mousavi [1,†], Arash Mousavi [1,†], Yashar Mousavi [2,*], Mahsa Tavasoli [3], Aliasghar Arab [4], Ibrahim Beklan Kucukdemiral [2] and Afef Fekih [5]

1 Department of Electrical Engineering and Applied Sciences, Paradise Research Center, Jahrom 7416813647, Iran; rashinmousavi66@gmail.com (R.M.); arash.mousavi@ieee.org (A.M.)
2 Department of Applied Science, School of Computing, Engineering and Built Environment, Glasgow Caledonian University, Glasgow G4 0BA, UK; ibrahim.kucukdemiral@gcu.ac.uk
3 Department of Applied Science & Technology, North Carolina A&T State University, Greensboro, NC 27411, USA; mtavasoli@aggies.ncat.edu
4 Department of Mechanical and Aerospace Engineering, New York University, New York, NY 10012, USA; aliasghar.arab@nyu.edu
5 Electrical and Computer Engineering Department, University of Louisiana at Lafayette, P.O. Box 43890, Lafayette, LA 70504, USA; afef.fekih@louisiana.edu
* Correspondence: seyedyashar.mousavi@gcu.ac.uk
† These authors contributed equally to this work.

Abstract: Quadrotor unmanned aerial vehicles (QUAVs) are widely recognized for their versatility and advantages across diverse applications. However, their inherent instability and underactuated dynamics pose significant challenges, particularly under external disturbances and parametric model uncertainties. This paper presents an advanced observer-based control framework to address these challenges, introducing a high-gain disturbance observer (HGDO) integrated with a neural-network-based adaptive fractional sliding mode control (NN-AFSMC) scheme. The proposed HGDO-NN-AFSMC ensures robust position and attitude tracking by effectively compensating for external disturbances and model uncertainties. A direct control approach is employed, significantly reducing computational complexity by minimizing the need for frequent online parameter updates while maintaining high tracking precision and robustness. The stability of the control system is rigorously analyzed using Lyapunov theory, and comprehensive simulation studies validate the proposed scheme's superior performance compared to other advanced control approaches, particularly in dynamic and uncertain operational environments. The proposed HGDO-NN-AFSMC achieves a position tracking error of less than 0.03 m and an attitude tracking error below 0.02 radians, even under external disturbances and parametric uncertainties of 20%. Compared to conventional robust feedback linearization (RFBL) and nonsingular fast terminal sliding mode control (NFTSMC), the proposed method improves position tracking accuracy by 25% and reduces settling time by approximately 18%.

Keywords: quadrotor UAV control; adaptive control; high-gain disturbance observer; neural-network-based control; external disturbance; model uncertainty

Citation: Mousavi, R.; Mousavi, A.; Mousavi, Y.; Tavasoli, M.; Arab, A.; Kucukdemiral, I.B.; Fekih, A. Observer-Based Adaptive Neural Control of Quadrotor Unmanned Aerial Vehicles Subject to Model Uncertainties and External Disturbances. *Actuators* **2024**, *13*, 529. https://doi.org/10.3390/act13120529

Academic Editor: Liang Sun

Received: 27 November 2024
Revised: 19 December 2024
Accepted: 20 December 2024
Published: 21 December 2024

1. Introduction

In recent years, quadrotor unmanned aerial vehicles (QUAVs) have garnered considerable attention from the engineering community due to their wide range of applications in both military and civilian sectors, including product delivery, emergency rescue missions, infrastructure inspection, surveillance, aerial photography, and mapping. The versatility of these applications relies on the QUAV's ability to hover stably, maneuver precisely, and maintain operational safety [1–3]. The key advantages of QUAVs include vertical take-off and landing capabilities, cost-effectiveness, simple manufacturing processes, and agile flight dynamics. In micro air vehicles (MAVs), a related category of aerial systems, significant advancements have also been achieved in their design and operation. MAVs, widely used for surveillance, environmental monitoring, and confined-space operations, rely on low Reynolds number aerodynamics characterized by unsteady phenomena such as vortex generation and wake interactions [4,5]. Biomimetic designs inspired by natural flyers, like cicadas, have further optimized MAV efficiency, leveraging flapping-wing mechanisms to improve lift and thrust [4]. These developments in MAV aerodynamics have served as inspirations for enhancing the adaptability and performance of other aerial systems. However, despite these benefits, the development of advanced control systems for QUAVs remains challenging due to their underactuated and coupled dynamics, as well as their sensitivity to external disturbances and model uncertainties [6]. Effective control technologies must, therefore, ensure that QUAVs can operate safely and efficiently, meeting the high standards for responsiveness and sustainability required by Industry 4.0. Addressing external disturbances and compensating for model uncertainties are essential to enhance QUAV stability and precision in real-world conditions. Without these robust mechanisms, QUAVs can be unstable, limiting their reliability in critical applications. As a result, studying advanced control methods focused on disturbance rejection and uncertainty compensation is vital for achieving consistent and reliable performance across a wide range of mission-critical scenarios.

The highly intricate and nonlinear nature of QUAV dynamics presents significant challenges in developing control systems that can effectively manage their operational complexities [7–9]. Existing control approaches, both linear and nonlinear, often depend on precise model parameters, which are challenging to measure accurately in practical settings, thereby complicating their deployment. Adaptive control methods, while designed to mitigate parameter uncertainties and respond to external disturbances, still face limitations in fully capturing the multifaceted dynamics of quadrotors [10]. Additionally, the inherent underactuation of quadrotors adds to these challenges, as it complicates precise position and attitude control, which are essential for stable and efficient operation. This need for adaptable and robust control methods for accurate tracking under uncertain conditions has driven considerable research interest in this area [11–15]. Addressing various issues such as sensor noise, model inaccuracies, unmodeled dynamics, and a range of external disturbances remains essential for effective control design [16–18]. A systematic analysis of different control techniques, including their strengths and limitations, is crucial in identifying the most efficient strategies for handling the uncertainties that affect QUAV performance. In this context, several studies offer innovative control strategies that handle model uncertainties and external disturbances effectively. For example, in [19], a geometric adaptive robust hierarchical control method was designed for underactuated quadrotors, minimizing the effects of nonlinearities, uncertainties, and dynamic coupling. Similarly, the authors in [20] proposed two adaptive robust control strategies—bounded adaptive control and asymptotic adaptive control—that stabilize the attitude of quadrotors even amid uncertain parameters, control input limitations, and external disturbances. These strategies ensure asymptotic stability by estimating key physical parameters, managing input saturation, and suppressing external disturbances. Additionally, [21] presented an approach for robust adaptive tracking control in quadrotors by combining a self-tuning regulator in the inner loop with a proportional–integral (PI) controller in the outer loop, resulting in improved robustness and tracking performance compared to the reference adaptive control model. Furthermore, in [16], a backstepping-based adaptive control framework was introduced to address parameter uncertainties, external disturbances, and sensor noise in QUAVs. This method avoids issues related to trigonometric singularities in Euler angles, maintains bounded estimation and tracking errors, and shows superior performance compared to proportional–integral–derivative (PID), standard backstepping, and geometric control approaches.

Advanced control methods, including neural network (NN)-based approaches and adaptive sliding mode control (SMC), have seen increased use to enhance the tracking precision of QUAVs [22–25]. The operational stability of quadrotors, however, is frequently compromised by external disturbances and inherent model uncertainties, which can lead to instability or even catastrophic failure in critical situations. This has driven extensive research into reliable control strategies that ensure QUAVs maintain stable performance and accurate tracking despite these external disturbances. For instance, in [26], a nonlinear observer-based SMC approach was developed specifically for QUAV control, with the nonlinear observer bolstering the robustness of the SMC to maintain effective trajectory tracking. In another study [27], an adaptive control scheme was developed that integrates a fast terminal SMC with NN capabilities to counteract external disturbances and model uncertainties. The scheme leverages NN for approximating unknown system dynamics and adaptive laws for estimating disturbance bounds, while fast terminal SMC accelerates convergence. Similarly, a nonsingular terminal SMC approach enhanced with state feedback and a disturbance observer (DO) was introduced for QUAV attitude control, effectively addressing external disturbances [28]. In [13], an adaptive fast-reaching nonsingular terminal SMC was designed for QUAVs to achieve rapid error convergence even in the face of model uncertainties and disturbances, outperforming traditional adaptive SMC in tracking accuracy and robustness. Further, a finite-time tracking control approach combined an NN-based control scheme with adaptive tuning for NN parameters and an auxiliary system to handle input saturation challenges, effectively addressing external disturbances and parametric uncertainties [29]. Another method, described in [30], uses learning-based robust tracking control that integrates a NN with an enhanced weight updating mechanism to handle time-varying and coupling uncertainties. This approach provides stable and accurate position and attitude tracking, demonstrating superior performance over conventional adaptive dynamic programming (ADP) and linear quadratic regulator (LQR) methods under varying disturbance conditions. Despite these advancements, several significant challenges persist within the literature. Many existing studies either simplified the complex dynamics of QUAVs or failed to address the full range of uncertainties encountered in real-world operations. Additionally, conventional methods often have a high computational overhead, which can restrict their use in real-time applications. These limitations underscore the pressing need for more robust, computationally efficient control strategies capable of managing the unpredictable and complex nature of QUAV operations effectively.

DO-based control has demonstrated efficacy in improving quadrotor trajectory tracking. However, many existing DOs are characterized by complex structures that increase the computational load on flight controllers [14,31–35]. While advancements in flight controller processing power have been significant, the high computational requirements associated with autonomous or semiautonomous flight operations—coupled with the inherent weight and power limitations of quadrotors—continue to constrain the available computing resources. Consequently, there is an ongoing demand for DOs that are both simple and computationally efficient. Additionally, these complex DOs often come with numerous tuning parameters, necessitating an intensive calibration process to achieve a rapid convergence rate [36–39]. Among the nonlinear observers, high-gain observers (HGOs) stand out for their simplicity and speed. HGOs utilize high gain to obtain state estimates, rapidly offering several beneficial attributes. First, their design and implementation are relatively straightforward, as they replicate the system model with a specific gain, the calculation of which is explicit. Second, HGOs are easy to tune through a single scalar design parameter, simplifying the tuning process. Lastly, they deliver global or semiglobal stability for a wide range of systems [40–42]. These advantageous features, however, come with a trade-off: conventional HGOs are susceptible to amplifying measurement noise, although recent designs have mitigated this issue. Building on the strengths of HGOs, their use in disturbance estimation has led to the development of high-gain disturbance observers (HGDOs) [43,44]. Despite their potential, HGDOs remain underexplored for quadrotor applications, particularly in real-world scenarios where measurement errors and external disturbances are prevalent.

Despite the advances in observer-based estimation, adaptive estimation, and neural network (NN)-based adaptive control for QUAVs, challenges persist in achieving robust performance without compromising design targets or imposing high computational demands on the system [45–47]. It remains critical to evaluate these methods systematically to identify their limitations and areas where further refinement is needed to address the complex control needs of QUAVs in practical applications. This study was driven by the goal of developing a more resilient and adaptive control strategy capable of handling the varied challenges QUAVs encounter in real-world environments. In response to the identified limitations of the existing approaches, this paper proposes an HGDO combined with an adaptive NN-based control strategy to estimate external disturbances and tackle modeling uncertainties efficiently while keeping computational overhead minimal. The primary contribution of this work lies in its adaptive control scheme, which was designed to maintain reliable system performance even under the influence of significant external disturbances. By leveraging NN-based approximations within the control framework, this approach achieves precise trajectory tracking across a wide range of operational conditions. The proposed methodology includes a nested NN-based adaptive sliding mode control (NN-AFSMC) strategy for controlling QUAVs. The control design prioritizes accurate position and attitude tracking and incorporates a direct approach that reduces computational complexity, enhancing robustness by limiting online parameter updates. This novel control scheme ensures that the quadrotor can execute tasks with high precision and reliability, making it adaptable to complex operational environments. Moreover, a key innovation of this method is the indirect integration of NNs within the adaptive SMC framework, which reduces the computational demands associated with real-time implementation. Unlike traditional direct NN-based methods that require the extensive online updating of NN parameters, the proposed approach simplifies the adaptation process by focusing on scalar virtual parameters instead of full vector updates. This design choice not only streamlines the control implementation but also strengthens system robustness, making it well suited for applications that demand high stability and adaptability in the presence of external disturbances. The contributions of this work to the current literature are summarized as follows:

- A comprehensive dynamic model of a QUAV is developed, addressing the limitations of previous studies that often relied on oversimplified models and neglected the intricate coupling between attitude and position dynamics.
- A novel integration of a high-gain disturbance observer (HGDO) and NN approximation capabilities with adaptive sliding mode control (AFSMC) is formulated to handle external disturbances and model uncertainties effectively. This approach retains the complexity of aerodynamic drag and other nonlinear effects, enhancing the control system's adaptability to realistic operational conditions.
- The proposed method introduces a virtual parameter concept, enabling the indirect use of neural networks, which substantially minimizes the need for frequent parameter updates. This results in a control approach that is not only computationally efficient but also structurally straightforward and cost-effective, ensuring the precise tracking of position and attitude.
- The robustness and disturbance tolerance of the proposed control strategy are validated against robust feedback linearization and nonsingular fast terminal sliding mode control approaches. Extensive simulations demonstrate the effectiveness of the approach under a variety of challenging conditions, underscoring its reliability and applicability in dynamic environments.

The remainder of this paper is structured as follows: Section 2 describes the problem statement by defining the QUAV model. Section 3 presents the developed high-gain disturbance observer. The proposed NN-AFSMC control scheme is investigated in Section 4, and the simulation results and respective discussions are provided in Section 4. Finally, Section 6 concludes this paper.

2. Detailed QUAV Model

This section presents the dynamic model of a QUAV used for delivery operations. The quadrotor, depicted in Figure 1, features four rotors, with rotors 1 and 3 rotating counterclockwise and rotors 2 and 4 rotating clockwise, whose specifications are illustrated in Table 1. These rotations generate control forces and moments, enabling flight maneuverability. The quadrotor dynamics are described using two coordinate systems: the inertial frame $\mathbb{E} = \{x_e, y_e, z_e\}$, which represents the global reference, and the body-fixed frame $\mathbb{B} = \{x_b, y_b, z_b\}$, attached to the vehicle. Assuming the quadrotor operates as a rigid body, the Newton–Euler equations are used to describe its motion.

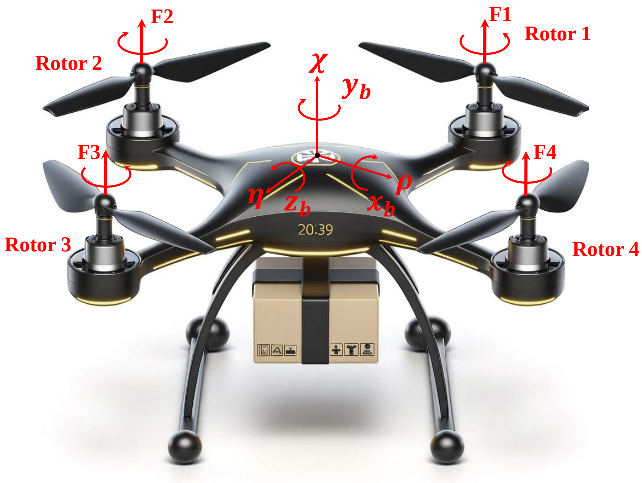

Figure 1. The configuration of a delivery quadrotor UAV.

The quadrotor's position in the inertial frame is denoted as $\omega = [x, y, z]^T \in \mathbb{R}^3$, and its orientation relative to the inertial frame is represented by Euler angles $\nu = [\rho, \chi, \eta]^T \in \mathbb{R}^3$. Concentrating on position control, the quadrotor's dynamics can be mathematically expressed as follows [16]:

$$
\begin{aligned}
\ddot{x} &= (\cos\rho\sin\chi\cos\eta + \sin\rho\sin\eta)\frac{T_{at}}{m} - \frac{\Phi_x\dot{x}}{m}, \\
\ddot{y} &= (\cos\rho\sin\chi\sin\eta - \sin\rho\cos\eta)\frac{T_{at}}{m} - \frac{\Phi_y\dot{y}}{m}, \\
\ddot{z} &= (\cos\rho\cos\chi)\frac{T_{at}}{m} - g - \frac{\Phi_z\dot{z}}{m}, \\
\ddot{\rho} &= \dot{\chi}\dot{\eta}\frac{I_y - I_z}{I_x} - \dot{\chi}\bar{\Theta}\frac{I_r}{I_x} - \frac{\dot{\rho}\Phi_\rho}{I_x} + \frac{\tau_{a\rho}}{I_x}, \\
\ddot{\chi} &= \dot{\rho}\dot{\eta}\frac{I_z - I_x}{I_y} - \dot{\rho}\bar{\Theta}\frac{I_r}{I_y} - \frac{\dot{\chi}\Phi_\chi}{I_y} + \frac{\tau_{a\chi}}{I_y}, \\
\ddot{\eta} &= \dot{\rho}\dot{\chi}\frac{I_x - I_y}{I_z} - \frac{\dot{\eta}\Phi_\eta}{I_z} + \frac{\tau_{a\eta}}{I_z}.
\end{aligned} \tag{1}
$$

where m represents the mass of the quadrotor, g is the gravitational acceleration, and $I = [I_x, I_y, I_z]$ are the moments of inertia. Aerodynamic damping effects are characterized by Φ_x, Φ_y, and Φ_z. The parameter I_r denotes the rotor inertia, and $\bar{\Theta} = \Theta_4 + \Theta_3 - \Theta_2 - \Theta_1$ captures the net angular momentum contribution from the rotors. The control thrust T_{at} and torques $\tau_{a\rho}$, $\tau_{a\chi}$, and $\tau_{a\eta}$ are expressed as

$$T_{at} = k(\Theta_1^2 + \Theta_2^2 + \Theta_3^2 + \Theta_4^2), \tag{2}$$

$$\tau_{a\rho} = kl(\Theta_3^2 - \Theta_1^2), \tag{3}$$

$$\tau_{a\chi} = kl(\Theta_4^2 - \Theta_2^2), \tag{4}$$

$$\tau_{a\eta} = b(\Theta_2^2 - \Theta_1^2 + \Theta_4^2 - \Theta_3^2), \tag{5}$$

where k is the thrust coefficient, b is the drag coefficient, and l is the distance from the rotor axis to the quadrotor's center of mass.

Table 1. Technical specifications of quadrotor blades and system.

Specification	Details	Unit
Chord length	0.254	m
Twist angle	−24 to 24	°C
Airfoil type	Wortmann FX63-137	–
Rotor diameter	0.3	m
Blade number	2	per rotor
Blade material	Carbon fiber	
Tip speed	80–100	m/s
Mechanism	Fixed pitch	–
Motor type	Brushless DC motors	–
Battery	11.1 Li-Po	V
Maximum payload	1	kg
Flight time	20–25	min
Weight	1.5–2	kg (including battery and payload)

Remark 1. *To ensure numerical stability and avoid singularities in the control model, the roll (ρ) and pitch (χ) angles are constrained to the interval $(-\frac{\pi}{2}, \frac{\pi}{2})$. This restriction eliminates issues at singular configurations such as $\chi = \pm\frac{\pi}{2}$ or $\rho = \pm\frac{\pi}{2}$.*

To design an effective control system for the QUAV, let the inputs from the rotors be defined as $u_1 = T_{at}$, $u_2 = \tau_{a\rho}$, $u_3 = \tau_{a\eta}$, and $u_4 = \tau_{a\chi}$. Based on the dynamic equations in (1), while accounting for the effects of external disturbances, $\delta_a(\cdot) = [\delta_x(\cdot), \delta_y(\cdot), \delta_z(\cdot)]^T \in \mathbb{R}^3$ and $\delta_b(\cdot) = [\delta_\rho(\cdot), \delta_\chi(\cdot), \delta_\eta(\cdot)]^T \in \mathbb{R}^3$, the translational dynamics $\dot{\omega}$ and rotational dynamics $\dot{p}$ can be reformulated as follows:

$$\ddot{\omega} = Au_{tr}(t) + \varpi_1(\cdot) + \delta_a(\omega, t), \tag{6}$$

$$\ddot{p} = Bu_r(t) + \varpi_2(\cdot) + \delta_b(p, t), \tag{7}$$

where $u_r = [u_2, u_3, u_4]^T$ and $u_{tr} = [U_x, U_y, U_z]^T$. Here, U_x, U_y, and U_z are the virtual control inputs for longitudinal, lateral, and altitude motion, respectively, defined as

$$\begin{aligned} U_x &= (\cos\rho \sin\chi \cos\eta + \sin\rho \sin\eta)u_1, \\ U_y &= (\cos\rho \sin\chi \sin\eta - \sin\rho \cos\eta)u_1, \\ U_z &= (\cos\rho \cos\chi)u_1. \end{aligned} \tag{8}$$

The matrices $A = \zeta_{12}\mathcal{I}^{3\times3}$ and $B = [\zeta_{13} \quad \zeta_{14} \quad \zeta_{15}]^T\mathcal{I}^{3\times3}$, along with the terms $\varpi_1(\cdot)$ and $\varpi_2(\cdot)$, are given by

$$\varpi_1(\cdot) = \begin{bmatrix} -\zeta_1\dot{x} \\ -\zeta_2\dot{y} \\ -\zeta_3\dot{z} - g \end{bmatrix}, \quad \varpi_2(\cdot) = \begin{bmatrix} \zeta_4\dot{\chi}\dot{\eta} - \zeta_9\dot{\chi}\bar{\Theta} - \zeta_6\dot{\rho} \\ \zeta_7\dot{\rho}\dot{\eta} - \zeta_8\dot{\rho}\bar{\Theta} - \zeta_5\dot{\chi} \\ \zeta_{10}\dot{\rho}\dot{\chi} - \zeta_{11}\dot{\eta} \end{bmatrix}.$$

The parameters ζ_i $(i = 1, \ldots, 15)$ are defined as

$$\zeta_1 = \frac{\Phi_x}{m}, \quad \zeta_2 = \frac{\Phi_y}{m}, \quad \zeta_3 = \frac{\Phi_z}{m}, \quad \zeta_4 = \frac{I_y - I_z}{I_x}, \quad \zeta_5 = \frac{\Phi_\chi}{I_y}, \quad \zeta_6 = \frac{\Phi_\rho}{I_x},$$

$$\zeta_7 = \frac{I_z - I_x}{I_y}, \quad \zeta_8 = \frac{I_r}{I_y}, \quad \zeta_9 = \frac{I_r}{I_x}, \quad \zeta_{10} = \frac{I_x - I_y}{I_z}, \quad \zeta_{11} = \frac{\Phi_\eta}{I_z}, \quad \zeta_{12} = \frac{1}{m},$$

$$\zeta_{13} = \frac{1}{I_x}, \quad \zeta_{14} = \frac{1}{I_y}, \quad \zeta_{15} = \frac{1}{I_z}.$$

The system consists of four motor-propeller actuators, each potentially influenced by unmeasurable factors. These factors can cause the actual actuator input, u_{ai}, to differ from the intended input, u_i. This relationship is expressed as

$$u_{ai} = u_i + \psi_i(t), \tag{9}$$

where $\psi_i(t)$ represents the unmeasurable, time-varying component of the control input, constrained within certain bounds. From this point forward, time dependence is omitted for simplicity.

By incorporating the actuator uncertainties from (9) into the dynamics of (6) and (7), the revised equations become

$$\ddot{\omega} = Au_{tr} + AK_\Theta \psi_1 + \varpi_1(\cdot) + \delta_a(\omega, t), \tag{10}$$

$$\ddot{p} = Bu_r + B\psi_r + \varpi_2(\cdot) + \delta_b(p, t), \tag{11}$$

where $\psi_r = [\psi_2, \psi_3, \psi_4]^T$, and K_Θ is a control matrix capturing the influence of the rotor angles:

$$K_\Theta = \begin{bmatrix} \cos\rho \sin\chi \cos\eta + \sin\rho \sin\eta \\ \cos\rho \sin\chi \sin\eta - \sin\rho \cos\eta \\ \cos\rho \cos\chi \end{bmatrix}.$$

Remark 2. *The quadrotor is an underactuated system, characterized by six degrees of freedom $(x, y, z, \rho, \chi, \eta)$ and four control inputs (u_1, u_2, u_3, u_4). By substituting the actual input u_1 with virtual control inputs U_x, U_y, and U_z, a control strategy can be devised in a manner analogous to that use for conventional systems.*

This work focused on developing an adaptive control strategy to address modeling uncertainties and external disturbances. The objective was to ensure that the system outputs $[x, y, z, \eta]$ closely track the desired reference trajectories $[x_d, y_d, z_d, \eta_d]^T$. The following assumptions form the basis for the proposed control framework:

Assumption 1. *The parameters $\zeta_1, \zeta_2, \ldots, \zeta_{15}$ are unknown but lie within bounded ranges. Additionally, ψ_i, representing unmeasurable and time-varying actuator uncertainties, is bounded and can change rapidly. Specifically, there exists an unknown scalar $\bar{\psi}$ such that $|\psi_i| \leq \bar{\psi} < \infty$.*

Assumption 2. *The desired position and orientation trajectories, denoted as $\omega_d, p_d, \dot{\omega}_d, \dot{p}_d, \ddot{\omega}_d, \ddot{p}_d$, are bounded. Moreover, the states of the system are assumed to be fully measurable and accessible for the control design.*

Assumption 3. *External disturbances, represented as δ_a and δ_b, are bounded such that $\|\delta_a\| \leq \bar{\delta}_1$ and $\|\delta_b\| \leq \bar{\delta}_2$, where $\bar{\delta}_1$ and $\bar{\delta}_2$ are unknown constants. The norm $\|\cdot\|$ refers to the $\mathcal{L}_1$ norm, defined as $\|\chi\| = \int_0^t |\chi(\alpha)|\, d\alpha$.*

Remark 3. *Accurately identifying system parameters is often infeasible due to the complexities of real-world operational conditions, making Assumption 1 both practical and necessary. Additionally,* *this assumption is widely utilized in managing actuator uncertainties [48]. Assumptions 2 and 3 are commonly adopted in tracking control problems for quadrotors to ensure the stability and robustness of the system [49,50].*

3. High-Gain Disturbance Observer

This section presents the design of an HGDO to estimate disturbances d_1 and d_2, denoted by their estimates $\hat{d}_1$ and $\hat{d}_2$. The proposed HGDO is formulated as follows:

$$\begin{cases} \dot{\hat{d}}_1 = \frac{1}{\epsilon_1}\left(d_1 - \hat{d}_1\right), \\ \dot{\hat{d}}_2 = \frac{1}{\epsilon_2}\left(d_2 - \hat{d}_2\right), \end{cases} \tag{12}$$

where $1/\epsilon_1$ and $1/\epsilon_2$ are the observer gains. Each equation in (12) represents a first-order filter with the transfer function $\frac{1}{\epsilon_i s+1}$.

Remark 4. *According to Assumption 3, Let us define the $j-$th component of d_i by d_i^j such that it satisfies*

$$\left\|d_i^j\right\| \le \delta_i^j. \tag{13}$$

The disturbances typically encompass unknown external forces, the gyroscopic effects of rotors, or aerodynamic influences such as drag. Although detailed models for gyroscopic and aerodynamic effects are available in the literature [51], these effects can be aggregated into disturbance terms for each axis. The HGDO is particularly advantageous as it estimates the amplitudes of such disturbances, thereby reducing the reliance on complex dynamic models.

By selecting small positive values for ϵ_i, the settling time of the observer is reduced, ensuring the rapid convergence of $\hat{d}_i$ to d_i. To express the system in state-space form, let us define the following variables: $x_1 = a$, $x_2 = \dot{a}$, $x_3 = b$, $x_4 = \dot{b}$, $d_1 = \frac{\delta_a}{m}$, $d_2 = \mathcal{I}^{-1}\delta_b$, $u_1 = \frac{K_\Theta u_1}{m}$, $u_2 = u_r[\zeta_{13}, \zeta_{14}, \zeta_{15}]^T$, $g = [0, 0, g]^T$, where $\mathcal{I}$ is the unit matrix. Additionally, let $\bar{K} = [\dot{\chi}\dot{\eta}\zeta_4, \dot{\rho}\dot{\eta}\zeta_7, \dot{\rho}\dot{\chi}\zeta_{10}]^T$. Using these definitions, the dynamics in (1) are rewritten as

$$\begin{cases} \dot{x}_1 = x_2, \\ \dot{x}_2 = -g + u_1 + d_1, \\ \dot{x}_3 = x_4, \\ \dot{x}_4 = \bar{K} + u_2 + d_2. \end{cases} \tag{14}$$

The unknown disturbances d_i can be extracted from (14) as

$$\begin{cases} d_1 = \dot{x}_2 + g - u_1, \\ d_2 = \dot{x}_4 - \bar{K} - u_2. \end{cases} \tag{15}$$

Based on these dynamics, the HGDO for the quadrotor is proposed as

$$\begin{cases} \dot{\hat{d}}_1 = \frac{1}{\epsilon_1}\left(\dot{x}_2 + g - u_1 - \hat{d}_1\right), \\ \dot{\hat{d}}_2 = \frac{1}{\epsilon_2}\left(\dot{x}_4 - \bar{K} - u_2 - \hat{d}_2\right). \end{cases} \tag{16}$$

Assuming that the initial disturbance estimates are zero, i.e., $\hat{d}_i(0) = 0$, the formulation in (16) has the drawback of amplifying measurement noise due to the inclusion of the derivatives of the system states. To address this issue, inspired by the approach in [52], auxiliary variables ξ_1 and ξ_2 are introduced:

$$\xi_1 = \hat{d}_1 - \frac{x_2}{\epsilon_1}, \quad \xi_2 = \hat{d}_2 - \frac{x_4}{\epsilon_2}. \tag{17}$$

The dynamics of these auxiliary variables are given as

$$\begin{cases} \dot{\xi}_1 = -\frac{1}{\epsilon_1}\left(\xi_1 + \frac{x_2}{\epsilon_1}\right) + \frac{1}{\epsilon_1}(g - u_1), \\ \dot{\xi}_2 = -\frac{1}{\epsilon_2}\left(\xi_2 + \frac{x_4}{\epsilon_2}\right) + \frac{1}{\epsilon_2}(-\bar{K} - u_2). \end{cases} \tag{18}$$

To establish the convergence properties of the observer, the disturbance estimation error is defined as $\tilde{d}_i = d_i - \hat{d}_i$. Differentiating $\tilde{d}_i$ and using (17) yields

$$\begin{cases} \dot{\tilde{d}}_1 = \dot{d}_1 - \left(\xi_1 + \frac{\dot{x}_2}{\epsilon_1}\right), \\ \tilde{d}_2 = \dot{d}_2 - \left(\xi_2 + \frac{\dot{x}_4}{\epsilon_2}\right). \end{cases} \tag{19}$$

Using the dynamics of (18) in (19), the disturbance estimation error dynamics can be expressed as

$$\dot{\tilde{d}}_i = -\frac{1}{\epsilon_i}\tilde{d}_i + \dot{d}_i. \tag{20}$$

The solution to this differential equation can be obtained by multiplying both sides by $e^{\frac{1}{\epsilon_i}t}$ and integrating over the interval $[0, t]$, resulting in

$$\tilde{d}_i(t) = \tilde{d}_i(0)e^{-\frac{1}{\epsilon_i}t} + \int_0^t e^{-\frac{1}{\epsilon_i}(t-\gamma)}\dot{d}_i(\gamma)d\gamma. \tag{21}$$

Rewriting (21) in a component-wise form and applying the absolute value operator gives

$$\left|\tilde{d}_i^j(t)\right| \leq \left|\tilde{d}_i^j(0)e^{-\frac{1}{\epsilon_i}t}\right| + \left|\int_0^t e^{-\frac{1}{\epsilon_i}(t-\gamma)}\dot{d}_i^j(\gamma)d\gamma\right|. \tag{22}$$

Using the triangle inequality [53], which states that $\left|\int_0^t \chi(v)dv\right| \leq \int_0^t |\chi(v)|dv$, one obtains

$$\left|\tilde{d}_i^j(t)\right| \leq \left|\tilde{d}_i^j(0)e^{-\frac{1}{\epsilon_i}t}\right| + \int_0^t \left|e^{-\frac{1}{\epsilon_i}(t-\gamma)}\dot{d}_i^j(\gamma)\right|d\gamma. \tag{23}$$

Integrating (23) over $[0, t]$ yields

$$\int_0^t \left|\tilde{d}_i^j(\gamma)\right|d\gamma \leq \int_0^t \left|\tilde{d}_i^j(0)e^{-\frac{1}{\epsilon_i}\gamma}\right|d\gamma + \int_0^t \left(\int_0^\tau e^{-\frac{1}{\epsilon_i}(\tau-\gamma)}\left|\dot{d}_i^j(\gamma)\right|d\gamma\right)d\tau, \tag{24}$$

where the first term on the right-hand side in (24) can be bounded as $\epsilon_i\left|\tilde{d}_i^j(0)\right|$. The second term is equivalent to $\left\|h(t) * \dot{d}_i^j(t)\right\|$, where $h(t) = e^{-t/\epsilon_i}$ and $*$ represent the convolution operator. Applying Young's convolution theorem [54], one has

$$\left\|h(t) * \dot{d}_i^j(t)\right\| \leq \|h(t)\|\left\|\dot{d}_i^j(t)\right\|. \tag{25}$$

Since the $\mathcal{L}_1$-norm of $h(t)$ is $\|h_i(t)\| = \epsilon_i$, it follows that

$$\int_0^t \left|\tilde{d}_i^j(\gamma)\right|d\gamma \leq \epsilon_i\left|\tilde{d}_i^j(0)\right| + \epsilon_i\left\|\dot{d}_i^j\right\|. \tag{26}$$

From the definition of the $\mathcal{L}_1$-norm and using (13), one obtains

$$\left\|\tilde{d}_i^j(t)\right\| \leq \epsilon_i\left(\left|\tilde{d}_i^j(0)\right| + \delta_i^j\right), \tag{27}$$

which leads to

$$\|\tilde{d}_i(t)\| \leq \epsilon_i\big(\|\tilde{d}_i(0)\| + \delta_i\big). \tag{28}$$

Since ϵ_i is a small positive constant, (28) demonstrates that the disturbance estimation error remains bounded and converges to a small value, verifying the effectiveness of the developed HGDO.

4. HGDO-NN-AFSMC Controller Design

In this section, an NN-AFSMC position and attitude control strategy is proposed for QUAVs based on an HGDO to address modeling uncertainties and external disturbances. Let us define the translational and rotational tracking errors as $e_\omega = \omega - \omega_d$ and $e_p = p - p_d$, respectively. To achieve robust tracking, two sliding surfaces are defined as

$$\begin{bmatrix} s_1 \\ s_2 \end{bmatrix} = \begin{bmatrix} v_1 e_\omega + \mathfrak{D}^{\lambda-1} e_\omega + \dot{e}_\omega \\ v_2 e_p + \mathfrak{D}^{\lambda-1} e_p + \dot{e}_p \end{bmatrix}, \tag{29}$$

where $\mathfrak{D}^\lambda(\cdot)$ denotes the Riemann–Liouville fractional derivative of order $0 < \lambda < 1$, and $v_1 > 0$ and $v_2 > 0$ are user-defined constants.

Taking the time derivative of (29) yields

$$\begin{bmatrix} \dot{s}_1 \\ \dot{s}_2 \end{bmatrix} = \begin{bmatrix} v_1 \dot{e}_\omega + \mathfrak{D}^\lambda e_\omega + A u_{tr} + A K_\Theta \psi_1 + \varpi_1(\cdot) + \delta_a - \ddot{\omega}_d \\ v_2 \dot{e}_p + \mathfrak{D}^\lambda e_p + B u_r + B \psi_r + \varpi_2(\cdot) + \delta_p - \ddot{p}_d \end{bmatrix}. \tag{30}$$

To simplify the analysis, the nonlinear terms are defined as

$$\begin{aligned} \bar{\mathcal{H}}_1(\cdot) &= v_1 \dot{e}_\omega + \mathfrak{D}^\lambda e_\omega + A K_\Theta \psi_1 + \varpi_1(\cdot) + \delta_a - \ddot{\omega}_d, \\ \bar{\mathcal{H}}_2(\cdot) &= v_2 \dot{e}_p + \mathfrak{D}^\lambda e_p + B \psi_r + \varpi_2(\cdot) + \delta_p - \ddot{p}_d. \end{aligned} \tag{31}$$

Both $\bar{\mathcal{H}}_1(\cdot)$ and $\bar{\mathcal{H}}_2(\cdot)$ consist of uncertain parameters and unmeasurable variables, making their direct inclusion in the control law impractical. Even if the analytical expressions for these terms were derived, incorporating them into the control design would increase the system's complexity and reduce the controller's flexibility.

Radial basis function NNs (RBFNNs), a subset of NNs, are widely recognized for their effectiveness in accurately approximating complex nonlinear functions, provided they are appropriately designed and configured [55–58]. This property can be leveraged to handle the nonlinearities and uncertainties encapsulated in $\bar{\mathcal{H}}_1(\cdot)$ and $\bar{\mathcal{H}}_2(\cdot)$. By employing RBFNNs, these terms can be approximated as

$$\begin{bmatrix} \bar{\mathcal{H}}_1(\cdot) \\ \bar{\mathcal{H}}_2(\cdot) \end{bmatrix} = \begin{bmatrix} w_1^{*T} \chi_1(\Omega_1) + \Phi_1(\Omega_1) \\ w_2^{*T} \chi_2(\Omega_2) + \Phi_2(\Omega_2) \end{bmatrix}, \tag{32}$$

where $\Omega_i = [\omega_i, \omega_{d,i}, \dot{\omega}_i, \dot{\omega}_{d,i}, \ddot{\omega}_i]$, $i = 1,2$ represents the input vector to the NN. The term $w_i^{*T} \in \mathbb{R}^n$ denotes the ideal weight vector, where n is the total number of neurons in the hidden layer. The terms Φ_i represent the approximation errors, and $\chi_i(\Omega_i)$ are the Gaussian activation functions defined as

$$\chi_i(\Omega_i) = \frac{1}{\sqrt{2\pi}\ell_i} \exp\left(-\frac{\|\Omega_i - \chi_i\|^2}{2\ell_i^2}\right), \quad i = 1,2, \tag{33}$$

where χ_i and ℓ_i are constants representing the center and width of the basis function, respectively.

It is important to note that both Φ_i and w_i^{*T} are bounded, satisfying $\|\Phi_i\| \leq \Phi_{m,i}$ and $\|w_i^{*T}\| \leq w_{m,i}$, where $\Phi_{m,i}$ and $w_{m,i}$ are unknown positive constants.

Theorem 1. *Considering the quadrotor's translational dynamics as outlined in (6), and assuming that Assumptions 1–3 hold true, the control algorithm is designed to guarantee that the tracking* *error e_ω remains ultimately uniformly bounded (UUB). By setting $\dot{s}_i = 0$, the control inputs for the translational and rotational subsystems can be expressed as $u_{tr} = -\frac{1}{A}\bar{\mathcal{H}}_1(\cdot)$ and $u_r = -\frac{1}{B}\bar{\mathcal{H}}_2(\cdot)$, respectively. The adaptive control law is then defined as*

$$\begin{bmatrix} u_{tr} \\ u_r \end{bmatrix} = \begin{bmatrix} -\frac{1}{A}\bar{\mathcal{H}}_1(\cdot) - (k_1 + 1/2)s_1 - \mathfrak{g}_1\hat{\beta}_1 s_1 \chi_1^2 \\ -\frac{1}{B}\bar{\mathcal{H}}_2(\cdot) - (k_2 + 1/2)s_2 - \mathfrak{g}_2\hat{\beta}_2 s_2 \chi_2^2 \end{bmatrix}, \tag{34}$$

with the adaptive law

$$\begin{bmatrix} \dot{\hat{\beta}}_1 \\ \dot{\hat{\beta}}_2 \end{bmatrix} = \begin{bmatrix} -\mu_1\hat{\beta}_1 + \mathfrak{g}_1\|s_1\|^2\chi_1^2 \\ -\mu_2\hat{\beta}_2 + \mathfrak{g}_2\|s_2\|^2\chi_2^2 \end{bmatrix}, \tag{35}$$

where $\hat{\beta}_i(0) \geq 0$, $k_i > 0$, $\mathfrak{g}_i > 0$, and $\mu_i > 0$ ($i = 1,2$) are user-specified design parameters. The variable $\hat{\beta}_i$ represents the estimate of β_i, defined as $\beta_i = w_{m,i}^2$.

Proof of Theorem 1. Applying the control law given in (34) results in the following closed-loop error dynamics:

$$\begin{bmatrix} \dot{s}_1 \\ \dot{s}_2 \end{bmatrix} = \begin{bmatrix} -(k_1 + 1/2)As_1 - A\mathfrak{g}_1\hat{\beta}_1 s_1\chi_1^2 \\ -(k_2 + 1/2)Bs_2 - B\mathfrak{g}_2\hat{\beta}_2 s_2\chi_2^2 \end{bmatrix}. \tag{36}$$

Given that the matrices $\{A, B\}$ are symmetric and positive-definite, the following inequalities hold: $s_1^T A s_1 \geq \kappa_a\|s_1\|^2$ and $s_2^T B s_2 \geq \kappa_b\|s_2\|^2$, where $0 < \kappa_a \leq \kappa_{\min}\{A\}$ and $0 < \kappa_b \leq \kappa_{\min}\{B\}$. Here, $\kappa_{\min}$ represents the smallest eigenvalue of the respective matrix. Consider the following Lyapunov function candidate,

$$\begin{bmatrix} V_1 \\ V_2 \end{bmatrix} = \begin{bmatrix} \frac{1}{2}s_1^T s_1 + \frac{1}{2\beta_1}\tilde{\beta}_1^2 + \frac{1}{2}\tilde{d}_1^T\tilde{d}_1 \\ \frac{1}{2}s_2^T s_2 + \frac{1}{2\beta_2}\tilde{\beta}_2^2 + \frac{1}{2}\tilde{d}_2^T\tilde{d}_2 \end{bmatrix}, \tag{37}$$

where $\tilde{\beta}_1 = \beta_1 - \kappa_a\hat{\beta}_1$ and $\tilde{\beta}_2 = \beta_2 - \kappa_b\hat{\beta}_2$ represent the virtual parameter estimation errors.

Using (32) and (36), the time derivative of $V_{1,2}$ can be expressed as

$$\begin{aligned} \begin{bmatrix} \dot{V}_1 \\ \dot{V}_2 \end{bmatrix} &= \begin{bmatrix} s_1^T\dot{s}_1 - \frac{\tilde{\beta}_1}{\beta_1}\dot{\hat{\beta}}_1 + \tilde{d}_1^T\dot{\tilde{d}}_1 \\ s_2^T\dot{s}_2 - \frac{\tilde{\beta}_2}{\beta_2}\dot{\hat{\beta}}_2 + \tilde{d}_2^T\dot{\tilde{d}}_2 \end{bmatrix} \\ &= \begin{bmatrix} s_1^T\left(-(k_1 + 1/2)As_1 - A\mathfrak{g}_1\hat{\beta}_1 s_1\chi_1^2 + w_1^{*T}\chi_1 + \Phi_1 + \tilde{d}_1\right) - \tilde{\beta}_1\dot{\hat{\beta}}_1 + \tilde{d}_1^T\dot{d}_1 - \tilde{d}_1^T\dot{\hat{d}}_1 \\ s_2^T\left(-(k_2 + 1/2)Bs_2 - B\mathfrak{g}_2\hat{\beta}_2 s_2\chi_2^2 + w_2^{*T}\chi_2 + \Phi_2 + \tilde{d}_2\right) - \tilde{\beta}_2\dot{\hat{\beta}}_2 + \tilde{d}_2^T\dot{d}_2 - \tilde{d}_2^T\dot{\hat{d}}_2 \end{bmatrix}. \end{aligned} \tag{38}$$

Applying the Young inequality, one obtains

$$\begin{bmatrix} s_1^T w_1^{*T}\chi_1 \leq \mathfrak{g}_1\beta_1\|s_1\|^2\chi_1^2 + \frac{1}{4\mathfrak{g}_1} \\ s_2^T w_2^{*T}\chi_2 \leq \mathfrak{g}_2\beta_2\|s_2\|^2\chi_2^2 + \frac{1}{4\mathfrak{g}_2} \end{bmatrix}, \tag{39}$$

$$\begin{bmatrix} s_1^T\Phi_1 \leq \frac{1}{2}\kappa_a\|s_1\|^2 + \frac{1}{2\kappa_a}\Phi_{m,1}^2 \\ s_2^T\Phi_2 \leq \frac{1}{2}\kappa_b\|s_2\|^2 + \frac{1}{2\kappa_b}\Phi_{m,2}^2 \end{bmatrix}, \tag{40}$$

$$\begin{bmatrix} s_1^T\tilde{d}_1 \leq \frac{1}{2}\|s_1\|^2 + \frac{1}{2}\|\tilde{d}_1\|^2 \\ s_2^T\tilde{d}_2 \leq \frac{1}{2}\|s_2\|^2 + \frac{1}{2}\|\tilde{d}_2\|^2 \end{bmatrix}. \tag{41}$$

By employing the adaptive law in (35) and substituting the inequalities from (39)–(41) into (38), the following expression is obtained:

$$
\begin{aligned}
\dot{V}_1 \leq & -(k_1+1/2)\kappa_a\|s_1\|^2 + \mathfrak{g}_1\tilde{\beta}_1\|s_1\|^2\chi_1^2 + \frac{1}{4\mathfrak{g}_1} \\
& + \frac{1}{2\kappa_a}\Phi_{m,1}^2 + \frac{1}{2}\kappa_a\|s_1\|^2 + \mu_1\tilde{\beta}_1\hat{\beta}_1 - \mathfrak{g}_1\tilde{\beta}_1\|s_1\|^2\chi_1^2 + \tilde{d}_1^T\dot{d}_1 - \tilde{d}_1^T\dot{\hat{d}}_1 \\
& \leq -k_1\kappa_a\|s_1\|^2 + \frac{1}{4\mathfrak{g}_1} + \frac{1}{2\kappa_a}\Phi_{m,1}^2 + \mu_1\tilde{\beta}_1\hat{\beta}_1 + \tilde{d}_1^T\dot{d}_1 - \tilde{d}_1^T\dot{\hat{d}}_1, \\
\dot{V}_2 \leq & -(k_2+1/2)\kappa_b\|s_2\|^2 + \mathfrak{g}_2\tilde{\beta}_2\|s_2\|^2\chi_2^2 + \frac{1}{4\mathfrak{g}_2} \\
& + \frac{1}{2\kappa_b}\Phi_{m,2}^2 + \frac{1}{2}\kappa_b\|s_2\|^2 + \mu_2\tilde{\beta}_2\hat{\beta}_2 - \mathfrak{g}_2\tilde{\beta}_2\|s_2\|^2\chi_2^2 + \tilde{d}_2^T\dot{d}_2 - \tilde{d}_2^T\dot{\hat{d}}_2 \\
& \leq -k_2\kappa_b\|s_2\|^2 + \frac{1}{4\mathfrak{g}_2} + \frac{1}{2\kappa_b}\Phi_{m,2}^2 + \mu_2\tilde{\beta}_2\hat{\beta}_2 + \tilde{d}_2^T\dot{d}_2 - \tilde{d}_2^T\dot{\hat{d}}_2.
\end{aligned} \tag{42}
$$

To enhance disturbance adaptation, an auxiliary parameter is introduced, defined as follows:

$$
\begin{bmatrix} \dot{\hat{d}}_1 \\ \dot{\hat{d}}_2 \end{bmatrix} = \begin{bmatrix} \dot{d}_1 - \bar{\xi}_1\tilde{d}_1 \\ \dot{d}_2 - \bar{\xi}_2\tilde{d}_2 \end{bmatrix}, \tag{43}
$$

where $\bar{\xi}_{1,2} > 0$ are constant gains introduced to ensure a reduction in the disturbance estimation error over time. By substituting (43) into (42) and utilizing the inequalities $0 < \mu_1\tilde{\beta}_1\hat{\beta}_1 \leq \mu_1\frac{1}{\kappa_a}(\beta_1^2 - \tilde{\beta}_1^2)$ and $0 < \mu_2\tilde{\beta}_2\hat{\beta}_2 \leq \mu_2\frac{1}{\kappa_b}(\beta_2^2 - \tilde{\beta}_2^2)$, (42) can be further simplified and expressed as

$$
\begin{aligned}
\dot{V}_1 &\leq -\left(k_1 + \frac{1}{2}\right)\kappa_a\|s_1\|^2 - \frac{\mu_1}{\kappa_a}\tilde{\beta}_1^2 - \bar{\xi}_1\|\tilde{d}_1\|^2 + \frac{1}{4\mathfrak{g}_1} + \frac{1}{2\kappa_a}\Phi_{m,1}^2 + \frac{\mu_1}{\kappa_a}\beta_1^2, \\
\dot{V}_2 &\leq -\left(k_2 + \frac{1}{2}\right)\kappa_b\|s_2\|^2 - \frac{\mu_2}{\kappa_b}\tilde{\beta}_2^2 - \bar{\xi}_2\|\tilde{d}_2\|^2 + \frac{1}{4\mathfrak{g}_2} + \frac{1}{2\kappa_b}\Phi_{m,2}^2 + \frac{\mu_2}{\kappa_b}\beta_2^2.
\end{aligned} \tag{44}
$$

Considering the constants $\Psi_1 = \frac{1}{4\mathfrak{g}_1} + \frac{1}{2\kappa_a}\Phi_{m,1}^2 + \frac{\mu_1}{\kappa_a}\beta_1^2 < \infty$ and $\Psi_2 = \frac{1}{4\mathfrak{g}_2} + \frac{1}{2\kappa_b}\Phi_{m,2}^2 + \frac{\mu_2}{\kappa_b}\beta_2^2 < \infty$, ensuring that the derivatives of the Lyapunov functions, $\dot{V}_{1,2}$, are strictly negative requires that the constants Ψ_1 and Ψ_2 satisfy the following condition:

$$
\begin{bmatrix} \Psi_1 \\ \Psi_2 \end{bmatrix} < \begin{bmatrix} \left(k_1 + \frac{1}{2}\right)\kappa_a\|s_1\|^2 + \frac{\mu_1}{\kappa_a}\tilde{\beta}_1^2 + \xi_1\|\tilde{d}_1\|^2 \\ \left(k_2 + \frac{1}{2}\right)\kappa_b\|s_2\|^2 + \frac{\mu_2}{\kappa_b}\tilde{\beta}_2^2 + \xi_2\|\tilde{d}_2\|^2 \end{bmatrix}. \tag{45}
$$

To ensure that $\dot{V}_{1,2} < 0$ regardless of the values of $\|s_i\|^2$, $\tilde{\beta}_i^2$, and $\|\tilde{d}_i\|^2$, $i = 1,2$, the constants $\Psi_{1,2}$ must satisfy the conditions

$$
\begin{cases}
\Psi_1 &= \frac{1}{4\mathfrak{g}_1} + \frac{1}{2\kappa_a}\Phi_{m,1}^2 + \frac{\mu_1}{\kappa_a}\beta_1^2 < 0, \\
\Psi_2 &= \frac{1}{4\mathfrak{g}_2} + \frac{1}{2\kappa_b}\Phi_{m,2}^2 + \frac{\mu_2}{\kappa_b}\beta_2^2 < 0.
\end{cases} \tag{46}
$$

Since these parameters are inherently positive, it becomes necessary to ensure that $\Psi_{1,2}$ are minimized relative to the chosen control gains $k_{1,2}$, $\mu_{1,2}$, and $\xi_{1,2}$ in the Lyapunov function. To achieve this, the control parameters $k_{1,2}$, $\kappa_{a,b}$, $\mu_{1,2}$, and $\xi_{1,2}$ must be selected such that $(k_1+1/2)\kappa_a$, $(k_2+1/2)\kappa_b$, μ_1/κ_a, μ_2/κ_b, and $\xi_{1,2}$ are sufficiently large to dominate $\Psi_{1,2}$. This ensures that the negative terms in $\dot{V}_{1,2}$ exceed the positive constants $\Psi_{1,2}$, resulting in a negative value for $\dot{V}_{1,2}$.

Furthermore, given that $\dot{V}_{1,2}$ are negative semidefinite and bounded, it follows that the Lyapunov functions $V_{1,2} \in \mathcal{L}_\infty$ are ultimately bounded, meaning $V_{1,2} \in \mathcal{L}_\infty$. The $\mathcal{L}_\infty$-norm is defined as the maximum absolute value, given by $\|x\|_\infty = \max_i |x_i|$ for a vector x, or $\|f\|_\infty = \sup_t |f(t)|$ for a function $f(t)$. Consequently, the boundedness of $V_{1,2}$ guarantees that the sliding variables $s_{1,2}$ are also bounded, implying $s_{1,2} \in \mathcal{L}_\infty$. Considering the bounded nature of $\dot{s}_1$, along with the boundedness of $\hat{\beta}_{1,2}$ and $\chi_{1,2}$, it can be inferred that:

$$\begin{bmatrix} \|\dot{s}_1\| \\ \|\dot{s}_2\| \end{bmatrix} \leq \begin{bmatrix} \left| k_1 + \frac{1}{2} \right| \|A\|\|s_1\| + \mathfrak{g}_1 \|\hat{\beta}_1\|\|s_1\|\|\chi_1\|^2 \leq G_1\|s_1\| + G_2, \\ \left| k_2 + \frac{1}{2} \right| \|A\|\|s_2\| + \mathfrak{g}_2 \|\hat{\beta}_2\|\|s_2\|\|\chi_2\|^2 \leq G_3\|s_2\| + G_4, \end{bmatrix}, \tag{47}$$

where $\{G_1, G_2, \ldots, G_4\}$ represent the constants determined by the maximum values of the bounded terms. Additionally, $\hat{\beta}_{1,2} \in \mathcal{L}_\infty$ is established due to the bounded nature of the adaptive law in (35). Since $\hat{\beta}_{1,2}$, $s_{1,2}$, and $\chi_{1,2}$ are confirmed to be bounded, it follows that

$$\begin{bmatrix} \|\dot{\hat{\beta}}_1\| \\ \|\dot{\hat{\beta}}_2\| \end{bmatrix} \leq \begin{bmatrix} \mu_1\|\hat{\beta}_1\| + \mathfrak{g}_1\|s_1\|^2\|\chi_1\|^2 \\ \mu_2\|\hat{\beta}_2\| + \mathfrak{g}_1\|s_2\|^2\|\chi_2\|^2 \end{bmatrix}. \tag{48}$$

Hence, $\dot{e}_\omega \in \mathcal{L}_\infty$, $e_\omega \in \mathcal{L}_\infty$, and $u_{atr} \in \mathcal{L}_\infty$. This indicates that all internal system signals are bounded. □

Remark 5. *The novelty of the proposed adaptation law lies in its streamlined structure, which prioritizes minimizing the computational complexity of online parameter updates while ensuring both stability and convergence. Instead of updating a high-dimensional weight matrix as in traditional NN-based control methods, this law focuses on a virtual scalar parameter. This scalar is governed by a carefully constructed Lyapunov function, guaranteeing system stability and the convergence of tracking errors to a small neighborhood around zero. Additionally, the adaptation law is designed to handle bounded uncertainties robustly, allowing the control system to adapt to real-time variations without significant computational overhead.*

By considering (8) and employing the trigonometric identity $\sin^2(\cdot) + \cos^2(\cdot) = 1$, it can be deduced that $u_1^2 = U_x^2 + U_y^2 + U_z^2$. Given that u_{tr} is defined as $u_{tr} = [U_x, U_y, U_z]^T$ and using the virtual control u_{tr} as formulated in (34), the actual control input u_1 can be determined directly as

$$u_1 = \|u_{tr}\| = \sqrt{U_x^2 + U_y^2 + U_z^2}. \tag{49}$$

Furthermore, the desired roll and pitch references, ρ_d and χ_d, are derived from the virtual position controller, as elaborated in [59]. According to (8), the system exhibits six degrees of freedom $\{\rho, \chi, \eta, U_x, U_y, U_z\}$. Here, U_x, U_y, and U_z are determined using (34), while the desired yaw trajectory η_d is predefined as an additional reference. Consequently, ρ_d and χ_d are calculated following the methodology in [59]:

$$\rho_d = \arcsin\left(\frac{U_x \sin(\eta_d) - U_y \cos(\eta_d)}{\|u_{tr}\|}\right), \tag{50}$$

$$\chi_d = \arctan\left(\frac{U_x \cos(\eta_d) + U_y \sin(\eta_d)}{U_z}\right). \tag{51}$$

It is worth noting that, to ensure the calculation of ρ_d and χ_d is singularity-free, three conditions must be satisfied. First, the magnitude of the virtual control vector, $\|u_{tr}\| = \sqrt{U_x^2 + U_y^2 + U_z^2}$, must be strictly positive ($\|u_{tr}\| > 0$) to prevent undefined values in the denominator of ρ_d. Second, the argument of the arcsin function, $\frac{U_x \sin(\eta_d) - U_y \cos(\eta_d)}{\|u_{tr}\|}$, must lie within the interval $[-1, 1]$ to ensure the arcsin function remains real-valued. Third, the denominator in χ_d, U_z, must not equal zero ($U_z \neq 0$) to avoid undefined results in the arctan function.

Remark 6. *The presented control strategy directly estimates the lumped uncertainties by leveraging NN capabilities. Unlike conventional approaches requiring online updates of a weight matrix w_i for each approximation, this method only updates scalar parameters (β_i). This significantly reduces computational complexity, especially for high-dimensional systems. The proposed framework simplifies neural adaptive control design while maintaining efficiency, as is further discussed in the subsequent sections.*

Remark 7. *The selection of hidden layer neurons in the NN strikes a balance between tracking accuracy and computational efficiency. Initially, a minimal number of neurons are selected, with increases made gradually until no significant improvement in tracking performance is observed. This methodology ensures optimal results without adding unnecessary complexity to the control system.*

Remark 8. *The parameters κ_a and κ_b play a pivotal role in stability analysis during the development of the controller. However, these parameters are not embedded within the control algorithm itself, removing the need for precise analytical predictions. This reduces computational overhead significantly. Furthermore, the control design does not depend on prior knowledge of lumped uncertainties $\bar{\mathcal{H}}_1(\cdot)$ and $\bar{\mathcal{H}}_2(\cdot)$. Once implemented, the control system does not require modifications or reprogramming, even under changing operational conditions for the QUAV (e.g., parameter variations or uncertainty bounds), as long as these changes remain within the assumed bounds specified in Assumptions 1 and 3.*

Remark 9. *The proposed framework integrates an HGDO with an online adaptive mechanism to estimate disturbances and approximate unknown uncertainties in real time. This approach addresses the unpredictable nature of disturbances and uncertainties, which renders pretraining impractical. The control strategy employs direct NN-based adaptive sliding mode control, focusing on virtual scalar parameters rather than requiring extensive online updates of large NN weight matrices. This design ensures robust, accurate control while meeting real-time requirements in dynamic and uncertain environments.*

5. Simulation Analysis

To validate the effectiveness and robustness of the proposed HGDO-NN-AFSMC controller, extensive simulation studies were conducted under challenging operating conditions. This section provides a detailed analysis of the simulation results, focusing on trajectory tracking performance and real-time computational efficiency.

5.1. Simulation Results

This section investigates the reliability of the proposed HGDO-based NN-AFSMC controller by evaluating the position and attitude-tracking capabilities across a spiral flight in the presence of external disturbances and model uncertainties. Table 2 illustrates the model parameters.

Table 2. Parameter settings for the quadrotor UAV.

Variable	Value	Unit
m	2.0	kg
g	9.81	m/s
l	0.2	m
k	$9.56E-6$	N·s^2
b	$1.14E-7$	N·s^2/rad^2
$\Phi_\rho, \Phi_\chi, \Phi_\eta$	$1.20E-6$	N·s/rad
Φ_x, Φ_y, Φ_z	$1.20E-2$	N·s/rad
I_x	0.75	N·s^2/rad
I_y	0.75	N·s^2/rad
I_z	1.50	N·s^2/rad

The performance of the proposed control approach for spiral trajectory tracking was compared against robust feedback linearization (RFBL) [60] and nonsingular fast terminal sliding mode control (NFTSMC) [61] under the influence of external disturbances and model uncertainties. The evaluation considered a spiral trajectory defined as $x_d = \cos(0.2t)$, $y_d = \sin(0.2t)$, and $z_d = 0.4t$, with a constant yaw path given by $\eta_d = 0$. To test robustness, variations in system parameters and external disturbances were introduced, including a 50% change in rotary inertia, a 25% change in aerodynamic drag coefficients, and external disturbances given by $\delta_a = [0.8\sin(t), 0.2\cos(t) + 0.4\sin(t), 2.1]^T$ and $\delta_b = [0.4 + 0.3\sin(8t), 0.75, 1.8 + 0.35\cos(40t)]^T$. The initial conditions for the system were set as $x_0 = (0.5, -0.5, 0)^T$ [m] for position and $p_0 = (0.2, 0.25, 0.2)^T$ [rad] for attitude. The parameters of the proposed HGDO-NN-AFSMC control scheme were defined as $\epsilon_{1,2} = 0.01$, $k_1 = 250$, $k_2 = 270$, $\mathfrak{g}_1 = \mathfrak{g}_2 = 0.2$, and $\mu_1 = \mu_2 = 0.7$. Additionally, the NN configuration included $n = 40$ neurons, a uniform NN center at $\chi_{1,2} = 0$, and a Gaussian function width of $\ell_{1,2} = 4$.

Remark 10. *The considered external disturbances, $\delta_a = [0.8\sin(t), 0.2\cos(t) + 0.4\sin(t), 2.1]^T$ and $\delta_b = [0.4 + 0.3\sin(8t), 0.75, 1.8 + 0.35\cos(40t)]^T$, incorporate low-frequency components ($\sin(t), \cos(t)$), high-frequency components ($\cos(40t)$), and constant biases. These configurations ensure the proposed controller's robustness under both gradual variations and rapid dynamic changes, which are often more challenging for conventional control schemes. The high-frequency component ($\cos(40t)$) approaches the upper threshold for practical quadrotor UAV studies, as actuator and aerodynamic limitations make disturbances beyond this range unrealistic. The adopted disturbances comprehensively tested the system's capability to handle uncertainty and rapid variations.*

Figure 2 illustrates the disturbance estimation performance of the HGDO for varying gain values. Among the examined configurations, the results indicate that $\epsilon = 0.05$ yields the most favorable disturbance estimation outcomes, characterized by superior convergence speed and minimal estimation error. Accordingly, the significant influence of ϵ on the accuracy and response time of the estimation process can be observed, highlighting its importance in effectively calibrating the disturbance observer to enhance performance. The control signals generated by the proposed approach are depicted in Figure 3, demonstrating that they remain uniformly bounded and continuous, which aligns with the theoretical analyses, ensuring the stability of the closed-loop system under varying operating conditions. As observed, when subjected to external disturbances and model uncertainties, the control signal amplitudes increase to counteract the adverse effects of these disturbances, ensuring robust system performance. This adaptive behavior highlights the ability of the HGDO-NN-AFSMC controller to compensate for uncertainties and maintain the desired system dynamics effectively. Additionally, the control signals exhibit minimal oscillations, indicating a smooth and efficient response to external disturbances, which is essential for practical applications involving precision.

Moreover, as depicted in Figures 4 and 5, the comparative analysis of rotational and translational trajectory tracking demonstrates that the proposed controller consistently surpasses the performance of the RFBL and NFTSMC approaches. In particular, the enhanced tracking precision of HGDO-NN-AFSMC is evident in the minimized deviation from the reference trajectory, even under significant disturbances. The improvement stems from the HGDO's ability to effectively estimate and compensate for external disturbances and the NN-AFSMC's adaptive nature, which dynamically adjusts to model uncertainties. As the zoomed-in insets illustrate, the proposed control scheme maintains a tighter adherence to the desired paths compared to the other methods during transitions and critical points such as the peaks and troughs of the references. Table 3 provides a detailed comparison of the mean attitude and rotational tracking errors for the three control approaches—RFBL, NFTSMC, and the proposed HGDO-NN-AFSMC—evaluated under external disturbances and model uncertainties during spiral flight. The results highlight that the proposed HGDO-NN-AFSMC achieves the lowest tracking errors across all rotational states (ρ, χ, μ) and translational coordinates (x, y, z), demonstrating its superior robustness and precision. Notably, the errors in the critical z-axis and yaw tracking (μ) are significantly reduced compared to RFBL and NFTSMC, showcasing the effectiveness of the HGDO in estimating disturbances and the NN-AFSMC's adaptive capability in handling uncertainties.

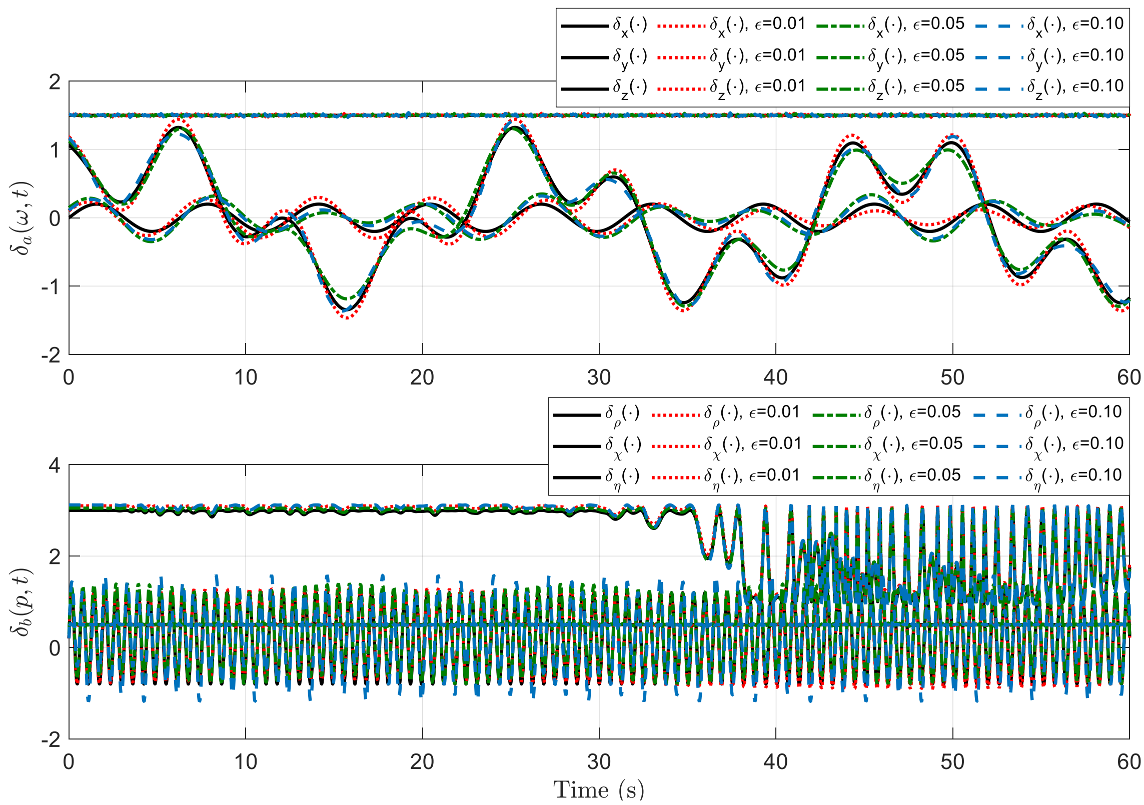

Figure 2. The imposed external disturbances on the QUAV and their estimations with different gains.

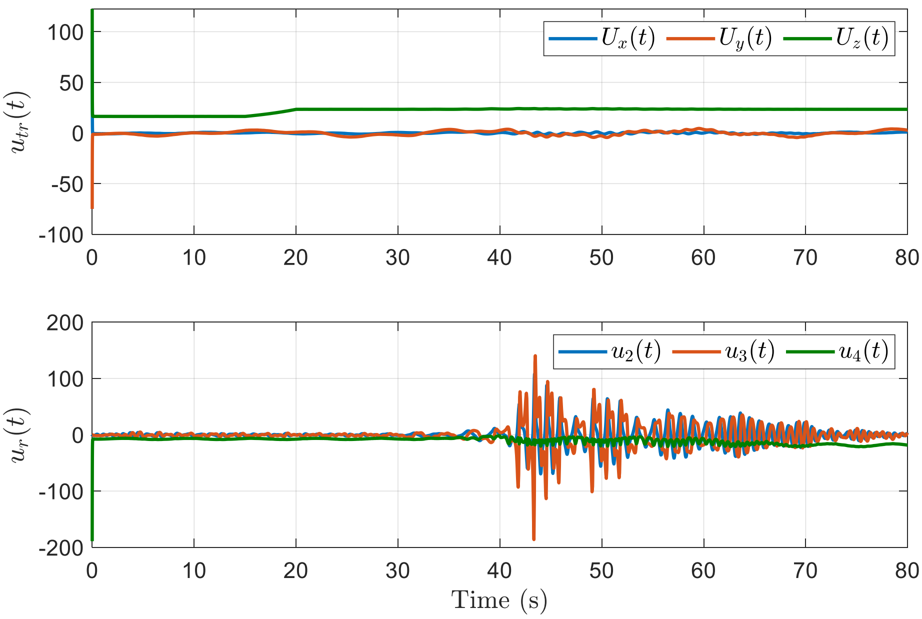

Figure 3. HGDO -NN-AFSMC control signals for the spiral flight tracking under external disturbances and model uncertainties.

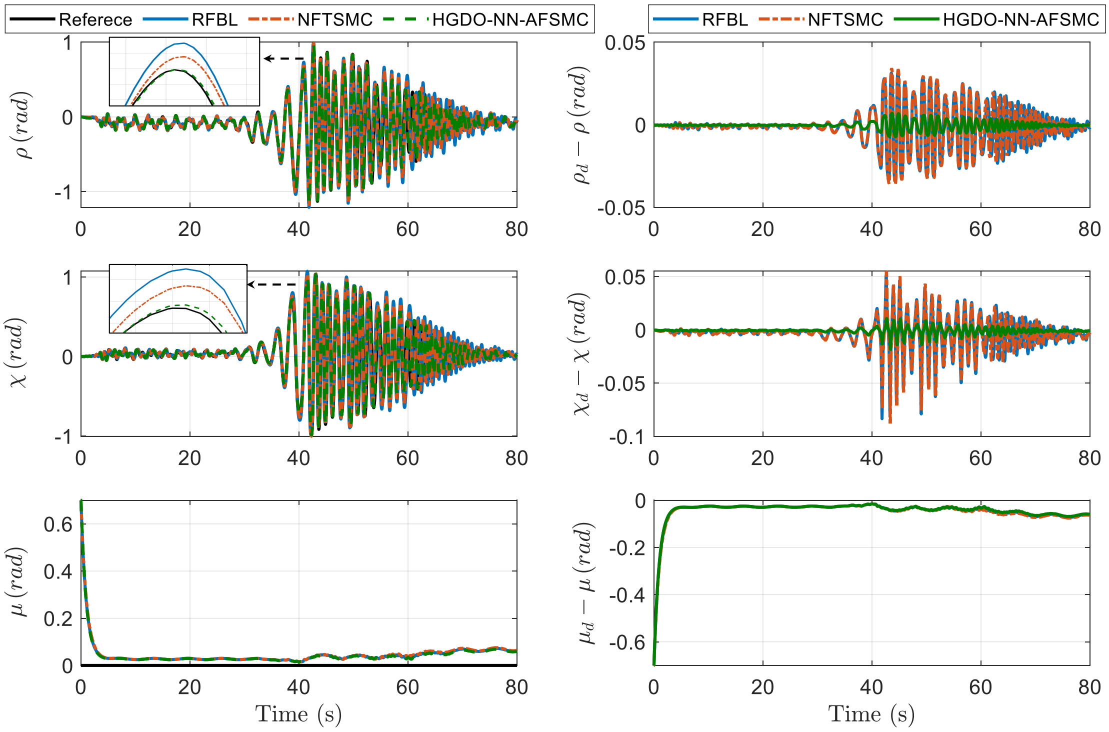

Figure 4. Comparative rotational tracking performance for the spiral flight under external disturbances and model uncertainties.

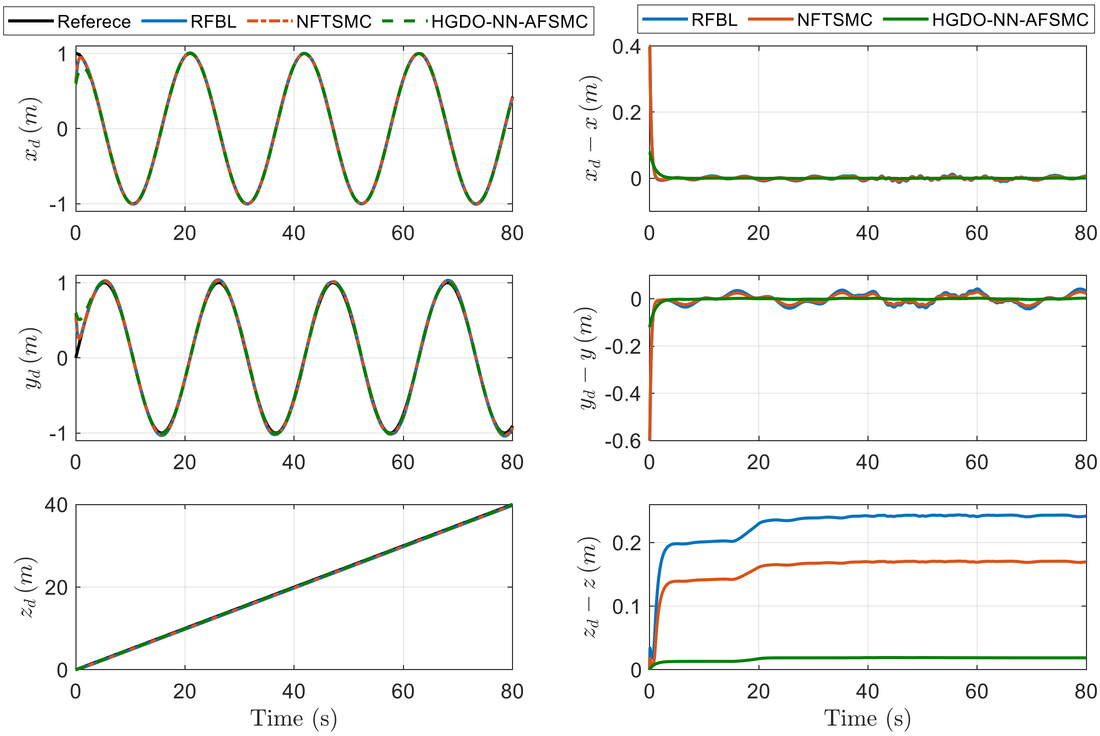

Figure 5. Comparative attitude tracking performance for the spiral flight under external disturbances and model uncertainties.

Table 3. Comparison of the mean tracking error performances under disturbances and uncertainties.

	Tracking Error (Mean)	RFBL	NFTSMC	HGDO-NN-AFSMC
Rotational	$\rho_d - \rho$ (rad)	0.0013	0.0012	0.0005
	$\chi_d - \chi$ (rad)	0.0035	0.0033	0.0015
	$\mu_d - \mu$ (rad)	0.0575	0.0516	0.0298
Attitude	$x_d - x$ (m)	0.0780	0.0741	0.0222
	$y_d - y$ (m)	0.0034	0.0033	0.0016
	$z_d - z$ (m)	0.2110	0.1513	0.0210

The 3D trajectory tracking performance, as shown in Figure 6, further validates the robustness of the HGDO-NN-AFSMC controller. While both the RFBL and NFTSMC approaches exhibit notable deviations from the reference path, the proposed method adheres closely to the desired trajectory, with errors confined within a significantly narrower margin. As observed, HGDO-NN-AFSMC consistently demonstrates higher fidelity in tracking the reference trajectories across all attitude states. This is largely due to the seamless integration of the HGDO and NN-AFSMC, which collectively enable the controller to handle high-frequency variations and abrupt trajectory changes with stability and precision. The HGDO-NN-AFSMC method closely follows the reference trajectories even during high-frequency variations or abrupt transitions, showcasing its robustness and precision. This superior tracking performance is a direct result of the combined effects of the external HGDO and the NN-AFSMC, which dynamically adjusts to uncertainties and disturbances.

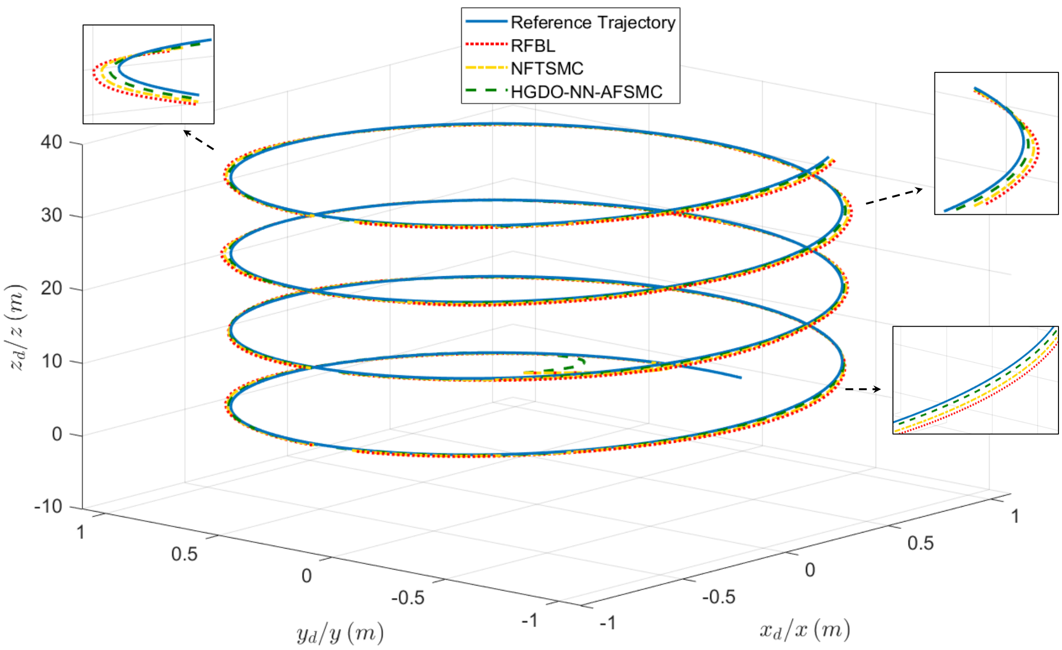

Figure 6. Comparative 3D tracking performance for the spiral flight under external disturbances and model uncertainties.

5.2. Real-Time Computational Analysis

This section provides a detailed analysis of the computational demands of the proposed HGDO-NN-AFSMC controller real-time requirements with respect to the RFBL and NFTSMC approaches. The computational structure of the proposed controller is streamlined through two key features:

- The HGDO estimates external disturbances using a first-order filtering mechanism (Equation (16)) with a single observer gain ϵ. This results in low computational complexity while ensuring rapid convergence and minimal estimation errors. As shown in Figure 2, $\epsilon = 0.05$ provides the best trade-off between accuracy and response time.

- Instead of updating the full NN weight matrix in real time, the proposed method leverages a virtual scalar parameter $\hat{\beta}_i$ (Equation (35)), which dramatically reduces the number of online computations compared to traditional adaptive neural controllers.

To quantify the real-time computational demands, simulations for a spiral trajectory were conducted on a standard machine with the following specifications: Intel i7-8700 CPU, 16 GB RAM, MATLAB R2023a. Table 4 summarizes the number of operations per loop and the corresponding computation times. As it is observed, the HGDO-NN-AFSMC achieves a favorable trade-off between computational complexity and robustness. Although RFBL has a slightly faster computation time (1.10 ms), its performance degrades significantly in the presence of large disturbances and model uncertainties (Section 5.1). Moreover, compared to NFTSMC, which incurs higher computational overhead due to its nonlinear terms and finite-time convergence dynamics, the proposed method offers 25% faster execution while maintaining superior tracking accuracy (Figures 4–6). In this context, the combination of HGDO for rapid disturbance estimation and NN-AFSMC for adaptive control ensures real-time implementation feasibility without sacrificing precision or robustness. As demonstrated, the proposed approach strikes an optimal balance between computational efficiency and tracking performance, making it ideal for dynamic and uncertain environments.

Table 4. Computational requirements of different control methods.

Method	Operations/Loop	Computation Time (ms)
HGDO-NN-AFSMC	$\sim$ 65 operations	1.85 ms
RFBL	$\sim$ 50 operations	1.10 ms
NFTSMC	$\sim$ 90 operations	2.45 ms

6. Conclusions

This study explored a robust control strategy for achieving precise position and attitude tracking in quadrotor UAVs under the influence of model uncertainties and external disturbances. A compound control framework was proposed, combining a high-gain disturbance observer (HGDO) with an adaptive neural-network-based fractional sliding mode control (NN-AFSMC) scheme. By leveraging a comprehensive and detailed dynamic model that captures the intricate nonlinear behaviors of QUAVs, the developed control scheme addresses the challenges of maintaining stable tracking performance in real-world operating conditions. A key novelty lies in the integration of virtual parameters with NNs, effectively reducing the number of online-updated parameters. This enhancement results in a control structure that is not only computationally efficient but also straightforward to implement, making it highly practical for real-time applications. The simplicity and adaptability of the proposed method ensure accurate position and attitude tracking without imposing significant computational demands. Theoretical analyses and extensive simulation studies confirmed the effectiveness of the proposed control approach. Additionally, the extensive simulations provided comparative results, demonstrating the ability of the HGDO-NN-AFSMC controller to outperform robust feedback linearization (RFBL) and nonsingular fast terminal sliding mode control (NFTSMC), especially under varying external disturbances and model uncertainties. These results emphasize the applicability of the proposed method in addressing real-world challenges for quadrotor UAV operations. The results demonstrate superior tracking accuracy and robustness compared to other advanced control methods in the presence of external disturbances and model uncertainties. These findings validate the potential of the HGDO-NN-AFSMC controller for practical applications requiring high precision and reliability in dynamic and uncertain environments.

In future work, experimental validation of the proposed control framework will be conducted to evaluate its practical applicability and robustness in real-world scenarios. In addition, advanced machine learning algorithms, such as reinforcement learning, can be integrated to dynamically adjust the control parameters in real- time based on the operational conditions and environmental changes to enhance the adaptability and robustness of the control scheme. Moreover, employing a hybrid control framework that integrates reinforcement learning with the existing HGDO-NN-AFSMC could allow the system to learn optimal control strategies while retaining the robust disturbance rejection capabilities of the current method. Furthermore, a study could leverage the capabilities of digital twins to provide a real-time, virtual replica of the QUAV system, enabling the continuous monitoring and simulation of various operational scenarios. In this context, the deployment of digital twins in conjunction with real QUAVs can facilitate extensive testing and fine-tuning of control schemes, ensuring they are well prepared for real-world challenges. This dual-testing methodology could also help identify potential implementation issues and accelerate the development of more efficient and reliable UAV control strategies. The combined approach of digital and physical testing can significantly enhance the reliability and efficiency of the developed approach. Additionally, while the proposed framework was specifically designed for quadrotor UAVs, its modular design and robust features make it applicable to a variety of other underactuated systems, such as robotic manipulators, marine vessels, or fixed-wing aircraft. Future studies can explore the generalization of this control framework to these domains by adapting the system dynamics and control parameters accordingly. For example, in robotics, the framework can be used to achieve precise trajectory tracking under uncertain payload conditions, while in aerospace applications, it can enhance stability and adaptability in challenging environmental conditions like high turbulence. Such generalizations will not only validate the versatility of the proposed method but also broaden its practical suitability in multiple disciplines.

Author Contributions: Conceptualization, R.M. and A.M.; methodology, R.M. and A.M.; software, R.M. and A.M.; validation, Y.M., M.T., and A.A.; formal analysis, Y.M.; investigation, R.M., A.M., and Y.M.; writing—original draft preparation, R.M. and A.M.; writing—review and editing, Y.M., M.T., A.A., I.B.K., and A.F.; supervision, Y.M., I.B.K., and A.F.; project administration, Y.M. All authors have read and agreed to the published version of this manuscript.

Funding: This research received no external funding.

Data Availability Statement: The data supporting the findings of this study are available from the corresponding author upon reasonable request, as the research is still ongoing.

Conflicts of Interest: The authors declare no conflicts of interest.

Abbreviations and Symbols

The following abbreviations, parameters, and symbols are used in this manuscript:

Abbreviations

3D	Three-Dimensional
ADP	Adaptive Dynamic Programming
DO	Disturbance Observer
FTSMC	Fast Terminal Sliding Mode Control
HGDO	High-Gain Disturbance Observer
LQR	Linear Quadratic Regulator
NFTSMC	Nonsingular Fast Terminal Sliding Mode Control
NN	Neural Network
NN-AFSMC	Neural Network-based Adaptive Fractional Sliding Mode Control
PID	Proportional–Integral–Derivative
QUAV	Quadrotor Unmanned Aerial Vehicle
RBFNN	Radial Basis Function Neural Network
RFBL	Robust Feedback Linearization
SMC	Sliding Mode Control
UAV	Unmanned Aerial Vehicle

Parameters and Symbols

a	System parameter	Φ_x, Φ_y, Φ_z	Translational aerodynamic damping coefficients
b	Drag coefficient	$\Phi_\rho, \Phi_\chi, \Phi_\eta$	Rotational aerodynamic damping coefficients
d	Distance between the rotors	ψ	Yaw angle
e_1, e_2, e_3	Position tracking errors	ψ_i	Actuator uncertainties
f_x, f_y, f_z	External forces acting on the quadrotor	ρ	Roll angle
g	Gravitational acceleration	τ	Torque
h	Height of the quadrotor	θ	Pitch angle
I_x, I_y, I_z	Quadrotor moments of inertia	v_1, v_2	Sliding surface design constants
J	Moment of inertia matrix	α	Adaptation gain
k	Thrust coefficient	β	Learning rate in NN
k_1, k_2	Sliding mode control gains	β_i	Virtual parameter for NN approximation
l	Rotor arm length (distance from center)	δ	Disturbance magnitude
m	Quadrotor mass	δ_a, δ_b	External disturbances
$\mathcal{I}$	Identity matrix	ϵ	Small positive constant
n	Number of neurons in NN	ϵ_i	Observer gain in HGDO
p	Orientation vector	η	Rotational aerodynamic damping coefficient
q	Quaternion components	γ_1, γ_2	Control gains
r	Rotor speed	κ	Control parameter for stability
s_1, s_2	Sliding surface variables	λ	Fractional derivative order
T_{at}	Total thrust force	μ_1, μ_2	Adaptive update rate constants
t	Time	ν	Adaptive parameter
u_1	Total thrust control input	Φ_i	NN approximation error
u_2, u_3, u_4	Control torques along roll, pitch, and yaw	x, y, z	Position coordinates in inertial frame
v_x, v_y, v_z	Velocities in the inertial frame	w_i^{*T}	Ideal NN weight vector

References

1. Hou, Y.; Chen, D.; Yang, S. Adaptive Robust Trajectory Tracking Controller for a Quadrotor UAV With Uncertain Environment Parameters Based on Backstepping Sliding Mode Method. *IEEE Trans. Autom. Sci. Eng.* **2023**, 1–11. [CrossRef]
2. Zhou, Z.; Hu, J.; Chen, B.; Shen, X.; Meng, B. Target Tracking and Circumnavigation Control for Multi-Unmanned Aerial Vehicle Systems Using Bearing Measurements. *Actuators* **2024**, *13*, 323. [CrossRef]
3. Hui, N.; Guo, Y.; Han, X.; Wu, B. Robust H-Infinity Dual Cascade MPC-Based Attitude Control Study of a Quadcopter UAV. *Actuators* **2024**, *13*, 392. [CrossRef]
4. Wan, H.; Dong, H.; Gai, K. Computational investigation of cicada aerodynamics in forward flight. *J. R. Soc. Interface* **2015**, *12*, 20141116. [CrossRef]
5. Wang, S.; Wang, S.; Fu, X.; Deng, X. A wall-boundary-natural transitional Reynolds-stress model for high-order wing-body simulations. *Phys. Fluids* **2024**, *36*, 084115. [CrossRef]
6. Liu, B.; Wang, Y.; Sepestanaki, M.A.; Pouzesh, M.; Mobayen, S.; Rouhani, S.H.; Fekih, A. Event-trigger-based adaptive barrier function higher-order global sliding mode control technique for quadrotor UAVs. *IEEE Trans. Aerosp. Electron. Syst.* **2024**, *60*, 5674–5684. [CrossRef]
7. Avram, R.C.; Zhang, X.; Muse, J. Nonlinear adaptive fault-tolerant quadrotor altitude and attitude tracking with multiple actuator faults. *IEEE Trans. Control. Syst. Technol.* **2017**, *26*, 701–707. [CrossRef]
8. Du, Y.; Huang, P.; Cheng, Y.; Fan, Y.; Yuan, Y. Fault tolerant control of a quadrotor unmanned aerial vehicle based on active disturbance rejection control and two-stage Kalman filter. *IEEE Access* **2023**, *11*, 67556–67566. [CrossRef]
9. Ke, C.; Cai, K.Y.; Quan, Q. Uniform passive fault-tolerant control of a quadcopter with one, two, or three rotor failure. *IEEE Trans. Robot.* **2023**, *39*, 4297–4311. [CrossRef]
10. Ramírez-Neria, M.; Luviano-Juárez, A.; González-Sierra, J.; Ramírez-Juárez, R.; Aguerrebere, J.; Hernandez-Martinez, E.G. Active Disturbance Rejection Control for the Trajectory Tracking of a Quadrotor. *Actuators* **2024**, *13*, 340. [CrossRef]
11. Ma, Q.; Jin, P.; Lewis, F.L. Guaranteed Cost Attitude Tracking Control for Uncertain Quadrotor Unmanned Aerial Vehicle Under Safety Constraints. *IEEE/CAA J. Autom. Sin.* **2024**, *11*, 1447–1457. [CrossRef]
12. Mallavalli, S.; Fekih, A. An Observer-based Backstepping Integral Nonsingular Fast Terminal Sliding Mode Fault Tolerant Control Design for Quadrotors Under Different Types of Actuator Faults. *Int. J. Control. Autom. Syst.* **2023**, *21*, 4015–4031. [CrossRef]
13. Mobayen, S.; El-Sousy, F.F.; Alattas, K.A.; Mofid, O.; Fekih, A.; Rojsiraphisal, T. Adaptive fast-reaching nonsingular terminal sliding mode tracking control for quadrotor UAVs subject to model uncertainties and external disturbances. *Ain Shams Eng. J.* **2023**, *14*, 102059. [CrossRef]
14. Mousavi, Y.; Zarei, A.; Mousavi, A.; Biari, M. Robust optimal higher-order-observer-based dynamic sliding mode control for VTOL unmanned aerial vehicles. *Int. J. Autom. Comput.* **2021**, *18*, 802–813. [CrossRef]
15. Liu, K.; Yang, P.; Wang, R.; Jiao, L.; Li, T.; Zhang, J. Observer-based adaptive fuzzy finite-time attitude control for quadrotor UAVs. *IEEE Trans. Aerosp. Electron. Syst.* **2023**, *59*, 8637–8654. [CrossRef]

16. Wang, J.; Zhu, B.; Zheng, Z. Robust adaptive control for a quadrotor UAV with uncertain aerodynamic parameters. *IEEE Trans. Aerosp. Electron. Syst.* **2023**, *59*, 8313–8326. [CrossRef]
17. Ma, W.; Hu, M.; Hao, W.; Wang, H.; Wang, P. Nonlinear Robust Fault-Tolerant Tracking Control of a Tri-Rotor UAV against Actuator's Abnormal Behavior. *Actuators* **2023**, *12*, 140. [CrossRef]
18. Arab, A.; Mousavi, Y.; Yu, K.; Kucukdemiral, I.B. Safety Prioritization by Iterative Feedback Linearization Control for Collaborative Robots. In Proceedings of the 2024 IEEE Conference on Control Technology and Applications (CCTA), Newcastle upon Tyne, UK, 21–23 August 2024; IEEE: Piscataway, NJ, USA, 2024; pp. 811–816.
19. Liang, W.; Chen, Z.; Yao, B. Geometric adaptive robust hierarchical control for quadrotors with aerodynamic damping and complete inertia compensation. *IEEE Trans. Ind. Electron.* **2021**, *69*, 13213–13224. [CrossRef]
20. Huang, T.; Li, T.; Chen, C.P.; Li, Y. Attitude Stabilization for a Quadrotor Using Adaptive Control Algorithm. *IEEE Trans. Aerosp. Electron. Syst.* **2023**, *60*, 334–347. [CrossRef]
21. Lei, W.; Li, C.; Chen, M.Z. Robust adaptive tracking control for quadrotors by combining PI and self-tuning regulator. *IEEE Trans. Control. Syst. Technol.* **2018**, *27*, 2663–2671. [CrossRef]
22. Yang, P.; Feng, K.; Ding, Y.; Shen, Z. Fast terminal sliding mode control based on finite-time observer and improved reaching law for aerial robots. *Actuators* **2022**, *11*, 258. [CrossRef]
23. Tashakkori, A.; Talebzadeh, M.; Salboukh, F.; Deshmukh, L. Forecasting gold prices with MLP neural networks: A machine learning approach. *Int. J. Sci. Eng. Appl.* **2024**, *13*, 13–20.
24. Dadkhah, D.; Moheimani, S.R. Combining H∞ and resonant control to enable high-bandwidth measurements with a MEMS force sensor. *Mechatronics* **2023**, *96*, 103086. [CrossRef]
25. Yang, P.; Wang, Z.; Zhang, Z.; Hu, X. Sliding mode fault tolerant control for a quadrotor with varying load and actuator fault. *Actuators* **2021**, *10*, 323. [CrossRef]
26. Ahmadi, K.; Asadi, D.; Merheb, A.; Nabavi-Chashmi, S.Y.; Tutsoy, O. Active fault-tolerant control of quadrotor UAVs with nonlinear observer-based sliding mode control validated through hardware in the loop experiments. *Control. Eng. Pract.* **2023**, *137*, 105557. [CrossRef]
27. Gao, B.; Liu, Y.J.; Liu, L. Adaptive neural fault-tolerant control of a quadrotor UAV via fast terminal sliding mode. *Aerosp. Sci. Technol.* **2022**, *129*, 107818. [CrossRef]
28. Nguyen, N.P.; Oh, H.; Moon, J. Continuous nonsingular terminal sliding-mode control with integral-type sliding surface for disturbed systems: Application to attitude control for quadrotor UAVs under external disturbances. *IEEE Trans. Aerosp. Electron. Syst.* **2022**, *58*, 5635–5660. [CrossRef]
29. Liu, K.; Wang, R.; Wang, X.; Wang, X. Anti-saturation adaptive finite-time neural network based fault-tolerant tracking control for a quadrotor UAV with external disturbances. *Aerosp. Sci. Technol.* **2021**, *115*, 106790. [CrossRef]
30. Mu, C.; Zhang, Y. Learning-based robust tracking control of quadrotor with time-varying and coupling uncertainties. *IEEE Trans. Neural Netw. Learn. Syst.* **2019**, *31*, 259–273. [CrossRef] [PubMed]
31. Mousavi, Y.; Zarei, A.; Kucukdemiral, I.B.; Fekih, A.; Alfi, A. Disturbance observer and tube-based model reference adaptive control for active suspension systems with non-ideal actuators. *IFAC-PapersOnLine* **2023**, *56*, 1075–1081. [CrossRef]
32. Dadkhah, D.; Moheimani, S.R. Design, Fabrication, and Control of a Double-Stage MEMS Force Sensor. *IEEE/ASME Trans. Mechatronics* **2024**, 1–11. [CrossRef]
33. Mousavi, Y.; Alfi, A.; Kucukdemiral, I.B.; Fekih, A. Tube-based model reference adaptive control for vibration suppression of active suspension systems. *IEEE/CAA J. Autom. Sin.* **2022**, *9*, 728–731. [CrossRef]
34. Arab, A.; Mousavi, Y. Optimal control of wheeled mobile robots: From simulation to real world. In Proceedings of the 2020 American Control Conference (ACC), Denver, CO, USA, 1–3 July 2020; IEEE: Piscataway, NJ, USA, 2020; pp. 583–589.
35. Shafai, B.; Zarei, F. Positive Stabilization and Observer Design for Positive Singular Systems. In Proceedings of the 2024 63rd IEEE Conference on Decision and Control (CDC), Milan, Italy, 16–19 December 2024; IEEE: Piscataway, NJ, USA, 2024.
36. Xu, S. Disturbance Observer-Based Adaptive Fault Tolerant Control with Prescribed Performance of a Continuum Robot. *Actuators* **2024**, *13*, 267. [CrossRef]
37. Mousavi, Y.; Bevan, G.; Kucukdemiral, I.B.; Fekih, A. Observer-based high-order sliding mode control of DFIG-based wind energy conversion systems subjected to sensor faults. *IEEE Trans. Ind. Appl.* **2023**, *60*, 1750–1759. [CrossRef]
38. Zarei, A.; Mousavi, Y.; Mosalanezhad, R.; Atazadegan, M.H. Robust voltage control in inverter-interfaced microgrids under plug-and-play functionalities. *IEEE Syst. J.* **2019**, *14*, 2813–2824. [CrossRef]
39. Xu, J.; Fang, L.; Wang, H.; Zhao, Q.; Wan, Y.; Gao, Y. Observer-Based Finite-Time Prescribed Performance Sliding Mode Control of Dual-Motor Joints-Driven Robotic Manipulators with Uncertainties and Disturbances. *Actuators* **2024**, *13*, 325. [CrossRef]
40. Sun, Z.; Liu, H.; Li, K.; Su, W.; Jiang, Y.; Chen, B. A Disturbance Observer-Based Fractional-Order Fixed-Time Sliding Mode Control Approach for Elevators. *Actuators* **2024**, *13*, 438. [CrossRef]
41. Mousavi, Y.; Bevan, G.; Kucukdemiral, I.B.; Fekih, A. Active fault-tolerant fractional-order terminal sliding mode control for dfig-based wind turbines subjected to sensor faults. In Proceedings of the 2022 IEEE IAS Global Conference on Emerging Technologies (GlobConET), Arad, Romania, 20–22 May 2022; IEEE: Piscataway, NJ, USA, 2022; pp. 587–592.
42. Xie, X.; Zheng, J.; Zhang, L. A Composite Control Method Based on Model Predictive Control and a Disturbance Observer for the Acquisition, Tracking, and Pointing System. *Actuators* **2024**, *13*, 417. [CrossRef]

43. Errouissi, R.; Viswambharan, A.; Shareef, H. Adaptive high-gain observer-based control for grid-tied LCL filter systems. *IEEE Trans. Ind. Appl.* **2023**, *59*, 5059–5073. [CrossRef]
44. Won, D.; Kim, W.; Tomizuka, M. Nonlinear control with high-gain extended state observer for position tracking of electro-hydraulic systems. *IEEE/ASME Trans. Mechatron.* **2020**, *25*, 2610–2621. [CrossRef]
45. Zhou, S.; Wang, M.; Jia, J.; Guo, K.; Yu, X.; Zhang, Y.; Guo, L. Fault Separation Based on An Excitation Operator with Application to a Quadrotor UAV. *IEEE Trans. Aerosp. Electron. Syst.* **2024**, *60*, 4010–4022. [CrossRef]
46. Rostam-Alilou, A.A.; Zhang, C.; Salboukh, F.; Gunes, O. Potential use of Bayesian Networks for estimating relationship among rotational dynamics of floating offshore wind turbine tower in extreme environmental conditions. *Ocean. Eng.* **2022**, *244*, 110230. [CrossRef]
47. Wang, H.; Cui, G.; Li, H. Fixed-time adaptive tracking control for a quadrotor unmanned aerial vehicle with input saturation. *Actuators* **2023**, *12*, 130. [CrossRef]
48. Wang, W.; Wen, C. Adaptive actuator failure compensation control of uncertain nonlinear systems with guaranteed transient performance. *Automatica* **2010**, *46*, 2082–2091. [CrossRef]
49. Zhao, B.; Xian, B.; Zhang, Y.; Zhang, X. Nonlinear robust adaptive tracking control of a quadrotor UAV via immersion and invariance methodology. *IEEE Trans. Ind. Electron.* **2014**, *62*, 2891–2902. [CrossRef]
50. Islam, S.; Liu, P.X.; El Saddik, A. Robust control of four-rotor unmanned aerial vehicle with disturbance uncertainty. *IEEE Trans. Ind. Electron.* **2014**, *62*, 1563–1571. [CrossRef]
51. Martini, S.; Sönmez, S.; Rizzo, A.; Stefanovic, M.; Rutherford, M.J.; Valavanis, K.P. Euler-Lagrange modeling and control of quadrotor UAV with aerodynamic compensation. In Proceedings of the 2022 International Conference on Unmanned Aircraft Systems (ICUAS), Dubrovnik, Croatia, 21–24 June 2022; IEEE: Piscataway, NJ, USA, 2022; pp. 369–377.
52. Won, D.; Kim, W.; Shin, D.; Chung, C.C. High-gain disturbance observer-based backstepping control with output tracking error constraint for electro-hydraulic systems. *IEEE Trans. Control. Syst. Technol.* **2014**, *23*, 787–795. [CrossRef]
53. Saitoh, S. Generalizations of the triangle inequality. *J. Inequal. Pure Appl. Math* **2003**, *4*, 5.
54. Carlen, E.A.; Lieb, E.H.; Loss, M. A sharp analog of Young's inequality on SN and related entropy inequalities. *J. Geom. Anal.* **2004**, *14*, 487–520. [CrossRef]
55. Zhao, W.; Gu, L. Adaptive PID Controller for Active Suspension Using Radial Basis Function Neural Networks. *Actuators* **2023**, *12*, 437. [CrossRef]
56. Tavasoli, M.; Lee, E.; Mousavi, Y.; Pasandi, H.B.; Fekih, A. Wipe: A novel web-based intelligent packaging evaluation via machine learning and association mining. *IEEE Access* **2024**, *12*, 45936–45947. [CrossRef]
57. Mousavi, A.; Mousavi, R.; Mousavi, Y.; Tavasoli, M.; Arab, A.; Fekih, A. Artificial Neural Networks-Based Fault Localization in Distributed Generation Integrated Networks Considering Fault Impedance. *IEEE Access* **2024**, *12*, 82880–82896. [CrossRef]
58. Zhang, C.; Feng, Y.; Wang, J.; Gao, P.; Qin, P. Vehicle sideslip angle estimation based on radial basis neural network and unscented Kalman filter algorithm. *Actuators* **2023**, *12*, 371. [CrossRef]
59. Islam, S.; Liu, P.; El Saddik, A. Nonlinear adaptive control for quadrotor flying vehicle. *Nonlinear Dyn.* **2014**, *78*, 117–133. [CrossRef]
60. Sadiq, M.; Hayat, R.; Zeb, K.; Al-Durra, A.; Ullah, Z. Robust Feedback Linearization based Disturbance Observer Control of Quadrotor UAV. *IEEE Access* **2024**, *12*, 17966–17981. [CrossRef]
61. Labbadi, M.; Cherkaoui, M. Robust adaptive nonsingular fast terminal sliding-mode tracking control for an uncertain quadrotor UAV subjected to disturbances. *ISA Trans.* **2020**, *99*, 290–304. [CrossRef]